AD-A051 992 PRATT AND WHITNEY AIRCRAFT GROUP EAST HARTFORD CONN F/G 20/11
BOUNDARY-INTEGRAL EQUATION METHOD FOR ELASTIC FRACTURE MECHANIC--ETC(U)
NOV 77 T A CRUSE, R B WILSON F44620-74-C-0060
UNCLASSIFIED PWA-5585 AFOSR-TR-78-0355 NL

| OF |
AD
A051992

END
DATE
FILMED
5-78
DDC

PWA-5585

(2)

BOUNDARY-INTEGRAL EQUATION METHOD FOR ELASTIC FRACTURE MECHANICS ANALYSIS

NOVEMBER 1977

FINAL SCIENTIFIC REPORT

T. A. CRUSE
R. B. WILSON

Pratt & Whitney Aircraft Group
United Technologies Corporation
East Hartford, Conn. 06108

PREPARED UNDER F44620-74-C-0060
FOR
AIR FORCE OFFICE OF SCIENTIFIC RESEARCH/NA
BUILDING 410, BOLLING AFB, D. C. 20332

UNCLASSIFIED

SECURITY CLASSIFICATION OF THIS PAGE (When Data Entered)

REPORT DOCUMENTATION PAGE

READ INSTRUCTIONS BEFORE COMPLETING FORM

1. REPORT NUMBER: AFOSR-TR-78-0355	2. GOVT ACCESSION NO.
3. RECIPIENT'S CATALOG NUMBER	
4. TITLE (and Subtitle): Boundary-Integral Equation Method for Elastic Fracture Mechanics Analysis	5. TYPE OF REPORT & PERIOD COVERED: Final rept. 1 April 1974 – 30 September 1977
6. PERFORMING ORG. REPORT NUMBER: PWA-5585	
7. AUTHOR(s): T. A. Cruse, R. B. Wilson	8. CONTRACT OR GRANT NUMBER(s): F44620-74-C-0060
9. PERFORMING ORGANIZATION NAME AND ADDRESS: Pratt & Whitney Aircraft Group, United Technologies Corporation, East Hartford, Connecticut 06108	10. PROGRAM ELEMENT, PROJECT, TASK AREA & WORK UNIT NUMBERS: [redacted] 2307-B1, 61102F
11. CONTROLLING OFFICE NAME AND ADDRESS: Air Force Office of Scientific Research/NA, Building 410, Bolling AFB, Washington, D. C. 20332	12. REPORT DATE: November 1977 13. NUMBER OF PAGES: 63p.
14. MONITORING AGENCY NAME & ADDRESS (if different from Controlling Office)	15. SECURITY CLASS. (of this report): UNCLASSIFIED 15a. DECLASSIFICATION/DOWNGRADING SCHEDULE

16. DISTRIBUTION STATEMENT (of this Report)

APPROVED FOR PUBLIC RELEASE
DISTRIBUTION UNLIMITED

17. DISTRIBUTION STATEMENT (of the abstract entered in Block 20, if different from Report)

18. SUPPLEMENTARY NOTES

19. KEY WORDS (Continue on reverse side if necessary and identify by block number)

Boundary-Integral Equation Method for Crack Analysis
Fracture Mechanics
Three-Dimensional Fracture Analysis
Inhomogeneous Fracture Mechanics
Stress Analysis
Numerical Analysis
Thermoelasticity

20. ABSTRACT (Continue on reverse side if necessary and identify by block number)

A review of recent progress in three-dimensional boundary-integral equation fracture mechanics analysis is presented. New results are discussed concerning the use of special crack tip elements in boundary-integral equation analysis.

A formulation is presented for the extension of boundary-integral equation analysis to materials with inhomogeneous material properties and to transient thermoelastic problems.

DD FORM 1 JAN 73 1473 EDITION OF 1 NOV 65 IS OBSOLETE

287 500

UNCLASSIFIED

SECURITY CLASSIFICATION OF THIS PAGE (When Data Entered)

FOREWORD

This is the Final Scientific Report prepared by the Pratt & Whitney Aircraft Group of United Technologies Corporation. The effort was sponsored by the Air Force Office of Scientific Research; (AFSC), United States Air Force, under Contract F44620-74-C-0060, project number 2307-B1, with Mr. W. J. Walker (NA) as Project Engineer. The period covered is April 1, 1974 through September 30, 1977.

Appreciation is expressed for the contributions made by Dr. L. H. Seitelman and Mr. D. W. Snow of Pratt & Whitney Aircraft during the final phase of the contract.

TABLE OF CONTENTS

LIST OF ILLUSTRATIONS

SECTION 1

INTRODUCTION

1.1 SUMMARY

The overall objective of this program has been the development of an analytical crack modeling and stress analysis capability, based on the boundary-integral equation method, of sufficient accuracy and efficiency to favorably influence the low cycle fatigue life prediction process for gas turbine engine structures. This report discusses progress toward this objective under the present contract, with particular attention to the period since the publication of the last Interim Scientific Report in May 1976.

The boundary-integral equation (BIE) method is known to be particularly well suited for the calculation of the rapidly varying stress fields associated with both fracture mechanics and stress concentration problems (Reference 1). During this program, the three-dimensional BIE method has been applied to a variety of fracture mechanics problems. The results of this work have been incorporated in the low cycle fatigue life prediction process. A new boundary-integral equation was derived for use in three-dimensional crack problems, which should significantly improve the ability to evaluate such finite geometry effects as the proximity of free surfaces or a condition of high local surface curvature. Most recently, modified BIE crack tip elements have been developed and applied to fracture mechanics problems.

The capabilities of the BIE method for stress analysis of uncracked gas turbine engine structures have been expanded by preliminary development of a technique for merging BIE and finite element analyses, by extension of the BIE method to deal with anisotropic and inhomogeneous materials, and by incorporation of thermal stresses in the BIE formulation.

Section 1.2 of this report is a brief overview of the BIE method; Section 1.3 discusses the application of the BIE method in the gas turbine engine environment. Section 2 is addressed specifically to the question of elastic fracture mechanics modeling, and Section 3 discusses application of the BIE method to inhomogeneous materials.

In addition to its impact on Pratt & Whitney Aircraft structural analysis efforts, the research carried out under this contract has been made widely available to the technical community through contract reports (References 2, 3, and 4), presentations at technical meetings, and publication in the open literature. References 5 through 9 discuss work fully or partially supported by this contract. In addition, the Appendix to this report has been accepted for publication in the International Journal for Numerical Methods in Engineering.

1.2 OVERVIEW OF THE BOUNDARY-INTEGRAL EQUATION METHOD

The BIE method for the solution of elastic stress analysis problems is based on classical results in mathematical analysis and continuum mechanics. It has become practical as a solution technique for problems with general geometry and loading because of the speed and storage capacity of present computers.

The analytical basis of the BIE method is the replacement, employing Betti's reciprocal work theorem, of the governing partial differential equations by an integral identity for the elastic displacements.

$$u_i(p) = \int_S T_{ij}(p,Q)\, u_j(Q)\, dS + \int_S U_{ij}(p,Q)\, t_j(Q)\, dS \qquad (1)$$

In Eq. (1), $u_i(p)$ is the displacement vector at an interior point $p(x)$; $t_i(Q)$ and $u_i(Q)$ are the boundary values of traction and displacement. The kernel functions $T_{ij}(p,Q)$ and $U_{ij}(p,Q)$ are the tractions and displacements in the x_i directions at $Q(x)$ due to orthogonal unit loads in the x_j directions at $p(x)$.

Equation (1) contains the totality of boundary data; in general, a well-posed elasticity problem consists of specifying values of t_j on part of the boundary, S_t and u_j on the remainder of the boundary S_u. Allowing $p(x) \rightarrow P(x)$, a boundary point, Eq. (1) becomes a set of integral constraint equations relating boundary displacements to boundary tractions; following References 10 and 11, the BIE is obtained.

$$u_i(P)/2 + \int_S T_{ij}(P,Q)\, u_j(Q)\, dS = \int_S U_{ij}(P,Q)\, t_j(Q)\, dS \qquad (2)$$

After the boundary solution u_j, t_j has been obtained, interior displacements can be calculated directly from Eq. (1). Interior stress can be evaluated by differentiation of Eq. (1) with respect to $p(x)$ and application of Hooke's Law. A detailed presentation of the analytical basis of the BIE method, including an extensive bibliography, was recently prepared (Reference 2) under support of this contract.

Solution of the analytical BIE, Eq. (2) is possible for only a few simple geometries and loadings. The practical application of the method is based on two approximations:

1. The boundary S of the region to be analyzed is represented by a finite number of surface patches, S_k. Examples are triangles in three dimensions and straight line segments in two dimensions.

2. The boundary data (u_i, t_i) are taken to have a known form of variation on each S_k; for example, linear variation over each individual S_k.

The first assumption allows the BIE to be rewritten as

$$\frac{u_i(P)}{2} + \sum_{k=1}^{N} \int_{S_k} T_{ij}(P,Q)\, u_j(Q)\, dS = \sum_{k=1}^{N} \int_{S_k} U_{ij}(P,Q)\, t_j(Q)\, dS \qquad (3)$$

Depending on the particular variation chosen for geometry variation and boundary data, the integrals over the surface patches are carried out either numerically (Reference 12) or in closed form (Reference 13) leading to a linear algebraic form of the BIE

$$[U]\ \{t\} = [T]\ \{u + \begin{bmatrix} \frac{1}{2} & 0 \\ 0 & \frac{1}{2} \end{bmatrix} \{u\} \tag{4}$$

Since the BIE in both its analytical and algebraic forms involves only boundary data, no interior idealization is required. The coefficient matrices in Eq. (4) are thus of much smaller order than those for a finite element analysis of the same problem, although they lack the banded structure of finite element coefficient matrices.

1.3 APPLICATION OF BIE STRESS ANALYSIS IN THE GAS TURBINE ENGINE ENVIRONMENT

BIE applications in the gas turbine engine environment fall into two major classes, fracture mechanics analysis (discussed in detail in Section 2) and calculation of elastic stress fields near notches and other structural details. This section is primarily addressed to the latter class, although many of the comments made also apply to the fracture mechanics problem.

1.3.1 *Geometrical Complexity*

The outstanding feature of problems encountered in gas turbine engine applications is geometrical complexity, leading to very large problem size. For example, the modeling of turbine disk rims involves such features as the load bearing teeth on the disk lug and the doubly curved surface at the rim slot/cooling hole intersection (Figure 1a).

The ability to model parts using the BIE method is strongly influenced by the way in which geometry and boundary data are allowed to vary over each surface patch. The BINTEQ program, used in much of the work carried out under this contract, uses plane triangular surface patches with linear boundary data variation (Reference 13). Modeling of a geometry such as a disk rim slot with BINTEQ requires use of a very large number of elements to obtain adequate definition (Figure 1b), leads to long computer run times, and makes the analysis unsuited to routine use.

An alternative (References 12 and 14) is the use of isoparametric shape functions for the representation of both geometry and boundary data. The basis of the isoparametric method is the mapping of a planar curve or a surface patch to a standard interval or square by means of a fixed set of shape functions. A particular set of quadratic shape functions is shown in Figure 2. In this case a surface patch defined by eight nodes (x^{α} , $\alpha = 1, \ldots, 8$) is mapped to the square ($-1 \leq \xi_1 \leq 1, -1 \leq \xi_2 \leq 1$) using the relation,

$$x_i(\xi) = M^{\alpha}(\xi)\, x_i^{\alpha} \tag{5}$$

The variation of $x_i(\xi)$ is quadratic along the edges of the square, although cubic terms can occur in the interior. Similar shape functions exist (Reference 14) for mapping of the triangle-like surface patches required for efficient mesh size transition. The improved modeling efficiency of the quadratic shape function approach (demonstrated for the rim slot/cooling

hole intersection in Figure 1b) allows the same level of solution accuracy to be achieved with a much less refined surface map. Other families of shape functions (linear and cubic) are discussed in Reference 12.

Boundary data can be modeled using the same representation as used for the geometry, the approach of Reference 14, or different representations can be allowed (Reference 12). The con bination of linear boundary data modeling with quadratic geometry representation is particularly attractive since it permits a low-cost, preliminary analysis of a complex part without sacrificing geometric definition. If the results of the preliminary analysis are satisfactory, then a more refined analysis can be carried out by improving the boundary data representation without changing the geometric representation. A different approach to the geometrical modeling problem is found in substructuring. Substructuring refers to the BIE modeling of a part in two or more separate subregions which are then joined by enforcing appropriate continuity conditions on the common elements which form the interfaces between subregions (Reference 12).

Pratt & Whitney Aircraft has acquired, for in-house use, a computer program (Reference 12), using the shape function approach and incorporating substructuring capability, referred to as BASQUE (Boundary Solution using Quadratic Elements).* This program has been used for much of the work carried out in the current part of the contract effort. Experience with the BASQUE code has shown that the increase in modeling efficiency due to the isoparametric approach and the substructuring capability permits practical three-dimensional BIE analysis of turbine disk rim and turbine blade attachment structures.

Finally, work has been carried out under this contract to explore the technique of hybridization, that is, the merging of BIE and finite element analysis. Some rather promising numerical results were achieved in the context of two-dimensional analysis. These results tegether with a discussion of more basic issues involved in coupling the BIE and finite element methods were reported in Reference 3 and 5.

1.3.2 Loading Complexity

Gas turbine engine structures experience loads other than the surface mechanical loads accounted for in Eq. (1). In particular, the structures are subjected to thermal, and often centrifugal loads. In order to account for these effects, the BIE must be modified to include the volume integrals of the body force terms for thermal and centrifugal loading. Since one of the advantages of the BIE method is the absence of an interior idealization, the existence of these volume integrals poses a difficult question.

During an earlier phase of this contract, a technique was developed for reducing the centrifugal body force volume integral to a surface integral. An exact reduction of the thermoelastic case to a surface integral was also obtained under the assumption of a steady state temperature field. Both analyses were incorporated in BINTEQ and verified numerically (Reference 4).

---

*This proprietary code was developed at the Centre Technique des Industries Mécaniques (CETIM) under the direction of Dr. J. C. Lachat. Further information about the code is available from M. Lange, Department Calcul des Structures, CETIM, BP 67, 60404 Senlis, France.

The surface integral reduction of the thermal loading was also studied as an approximate technique in the case of time dependent temperature fields but was found to be unsuitable for even small departures from steady state conditions. This is of considerable importance since, typically, engine structures must be analyzed at several points during an engine operating cycle, and the temperature fields at most or all of these points result from nonsteady state conditions. An alternative approach for BIE analysis of parts subjected to nonsteady state thermal loads is discussed in Section 3.

1.3.3 Material Complexity

Two types of complexity arise in the specification of elastic material properties for gas turbine engine structures: anisotropy and inhomogeneity.

Anisotropy results from the search for new materials which will have longer service lives under the increasingly demanding operating conditions found in advanced engines. It has been found that the use of anisotropic materials (particularly directionally solidified and single crystal materials in turbine airfoils) allows optimization of preferred material directions with respect to part loadings.

Anisotropy poses no problem in the formulation of Eq. (2), and integral representations for the required three-dimensional point load functions were established in References 15 and 16; however, efficient numerical evaluation of these point load functions posed a considerable problem. During the present contract, a technique was developed for minimizing this numerical problem. The technique was incorporated in the BASQUE code for verification and study of computational efficiency. A detailed description of this work is contained in the Appendix of this report.

Inhomogeneity of elastic material properties in gas turbine engine parts normally arises from the combination of temperature-dependent material properties and the fact that parts are subjected to nonuniform temperature fields. This problem is closely tied to the nonsteady state thermal body force problem mentioned above. One aspect of the present contract activity was the study of methods for dealing with these problems in the context of BIE analysis. The results of this study are discussed in Section 3.

SECTION 2

ELASTIC FRACTURE MECHANICS MODELING

2.1 INTRODUCTION

Gas turbine engine disk structures are often life limited due to the growth of fatigue cracks. Such cracks have been found to fall into two classes: subsurface or buried cracks originating from intrinsic defects and surface cracks initiated by fatigue loading of initially defect-free structural notches. The techniques of stress analysis and fracture mechanics have allowed reliable and conservative fatigue life prediction for buried cracks, and, combined with appropriate process control and inspection methods, have allowed satisfactory low cycle fatigue (LCF) lives to be achieved for structures with buried defects. The LCF life prediction problem for surface cracks is considerably more complex. Until recently, the complexity of both the crack geometry and the stress field near structural details, such as rim slots and bolt holes, has precluded the use of linear elastic fracture mechanics to predict propagation life for surface cracks. As a result, the fatigue life of structural details with stress concentrations was conservatively estimated by predicting the number of cycles to initiate a surface flaw of some specified size and ignoring the remaining propagation life.

The practical extension of elastic fracture mechanics techniques to the prediction of propagation of surface (including corner) cracks is based on the use of the weight function technique originally developed for two-dimensional problems (Reference 17). Development of an appropriate geometrical model for the surface crack has allowed extension of the weight function technique to three-dimensional problems (Reference 18). The crack modeling studies and the basic improvements in three-dimensional crack modeling capability carried out under the present contract have allowed the development at Pratt & Whitney Aircraft of an extensive stress intensity factor data base, calibrated with surface crack growth data.

Further, the generally improved capability for calculation of stress concentrations in complex structural details using the boundary-integral equation (BIE) method, which has been developed both under this contract and under Pratt & Whitney Aircraft in-house programs, has a direct impact on both the initiation and propagation problems for surface flaws. The system for the prediction of LCF cycles to surface flaw initiation is based in part on knowledge of the local concentrated stress. In addition, this local stress field in the uncracked part is used in the weight function method for the calculation of propagation life.

2.2 PREDICTION OF PROPAGATION LIFE FOR SURFACE FLAWS

2.2.1 The Weight Function Method

It has been shown in Reference 17 that for a linear-elastic body in plane strain loaded symmetrically about a crack, the Mode 1 stress-intensity factor for any load system can be calculated if the stress distribution in the uncracked body is known and the stress-intensity factor and displacement field are known for a single load state. In particular, in the absence of body forces

$$K^{(2)}(\ell) = \frac{H}{2K^{(1)}(\ell)} \int_{\Gamma} t^{(2)} \times \frac{\partial u^{(1)}}{\partial \ell} \, d\Gamma \tag{6}$$

where $K^{(2)}$ and $t^{(2)}$ are the stress-intensity factors and surface tractions of Load State 2 and $u^{(1)}$ is the displacement field for Load State 1. H denotes an appropriate elastic modulus for plane stress or plane strain, and ℓ is the crack length.

In the case mentioned previously, the crack is one dimensional, and its stress singularity is defined by a single stress-intensity factor. In the case of a crack in a three-dimensional geometry, the stress-intensity factor is a function of position on the crack face. In principle, the stress-intensity factor for any load state can be determined in a manner analogous to Eq. (6). In practice, the determination of the required information on variations of $u^{(1)}$ with crack geometry is too difficult.

In order to exploit the weight-function method in three-dimensional problems, it is necessary to reduce the number of degrees of freedom defining the crack shape. Service and experimental experience (References 6, 7, and 19) have shown that surface and corner cracks tend to have a part elliptical shape of rather moderate aspect ratio throughout their propagation life. This makes plausible an approach in which two degrees of freedom (the semiaxes a and b) are allowed to determine the ellipitcal crack shape. This approach (followed in Reference 18) allows the definition of the averaged stress intensity factors $\bar{K}_a$ and $\bar{K}_b$, which are weighted averages of the stress intensity factor distribution along the crack front. $\bar{K}_a$ and $\bar{K}_b$ are then related by the material crack growth model to independent growth of the two axes of the elliptical crack. In the two degree of freedom model this procedure leads to a coupled pair of ordinary differential equations for crack growth, since each $\bar{K}$ depends on the current shape of the crack.

Practical application of this two degree of freedom model requires an efficient method for evaluating $\bar{K}_a$ and $\bar{K}_b$ for various load states and ellipse aspect ratios. Equations similar to Eq. 6 allow evaluation of $\bar{K}_a$ and $\bar{K}_b$ for an arbitrary load state if $\partial W/\partial A|_a$ and $\partial W/\partial A|_b$ are known for a single reference load state. W is crack opening displacement and A is crack area. Calculation of these quantities requires solution of three-dimensional fracture mechanics problems and is too expensive for routine use. As an alternative, a data base has been set up, using three dimensional BIE analysis, in which are stored the required data for buried, surface and corner cracks in a bar of rectangular cross section for a variety of ellipse aspect ratios and bar thicknesses. Interpolation using this data allows efficient calculation of $\bar{K}_a$ and $\bar{K}_b$ for arbitrary aspect ratios and thicknesses.

2.2.2 Fracture Mechanics Calculations for Surface Cracks

Several different strategies have been explored in recent years for BIE modeling of cracked three-dimensional structures. The more general approach is to model the exterior of the cracked body and the crack surface, but not the unbroken region ahead of the crack, in which the traction distribution is singular. This modeling technique is applicable without symmetry restrictions on either geometry or loading. The first approach along this line was

the idealization of the crack as an open notch. Useful results were obtained with this technique (Reference 20), but it poses a major dilemma. The accuracy of the results suffers if the notch is too thick, that is if the (coincident) upper and lower surfaces of the mathematical crack are modeled too far apart. On the other hand, the equation system becomes badly conditioned if the surfaces are too close to one another.

One way to avoid these modeling difficulties is the development of a new mathematical formulation which allows modeling of both crack surfaces in the same plane without producing a singular BIE coefficient matrix. During the first phase of this contract, a new BIE was developed for three-dimensional bodies containing a buried plane crack of arbitrary shape (Reference 4). The displacement interpolation functions of the only three-dimensional BIE code (BINTEQ) available at that time were not smooth enough to allow implementation of the new BIE. The new BIE, in conjunction with the higher order BIE codes now available (References 12 and 14) can provide the closest analogy in three-dimensions to the exact two-dimensional mathematical crack modeling capability of the BIE/CRX code (Reference 21).

An alternative approach to three-dimensional fracture mechanics modeling proceeds from the observation that, in gas turbine engine structures, fatigue cracks normally grow in mode I, normal to an applied tension field. This observation suggests using the crack plane as a modeled symmetry plane, avoiding both problems associated with the open notch model. This modeling strategy was studied extensively during the first phase of the contract. Calculations were carried out, using the BINTEQ code, for buried, surface, and corner cracks modeled as ellipses or part-ellipses. The modeling strategy employed, data reduction procedures developed, and results obtained are discussed fully in References 4 and 7. The results obtained were also calibrated against experimentally derived mode I stress-intensity factor data for a growing surface flaw (Reference 6). Finally, fracture mechanics data obtained using this modeling approach has been used, in combination with the weight function method, to calibrate externally generated fatigue life data for corner cracks (References 6 and 19).

The work cited above has been shown to lead to satisfactory predictions of fatigue crack growth for design system purposes. The remaining questions center in two areas:

1. Interaction of part geometry with crack growth. The improved modeling efficiency of higher order BIE codes such as BASQUE will allow resolution of such effects.

2. Improved efficiency and absolute accuracy of BIE calculations in the near crack tip region. This characteristic becomes of particular importance in the study of the crack/free surface intersection. Work conducted as part of the current contract has been devoted to the development and evaluation of modified BIE crack tip elements. This work is discussed in Section 2.3.

2.3 USE OF BIE SINGULARITY EMEMENTS

2.3.1 The Modified BIE Crack Tip Element

The use of the symmetrical crack modeling strategy for mode I loading requires the approximation of near crack tip displacements and tractions in terms of the BIE interpolation functions. Considering a straight crack front, the variation of both displacement and traction is linear in r (distance from the crack front) in BINTEQ. In the BASQUE code, if midpoint nodes are placed at the geometrical midpoints of the element sides, the boundary data variation is quadratic in r. Since the near crack tip variation of the crack opening displacements is $\sqrt{r}$ and the normal traction variation ahead of the crack is $1/\sqrt{r}$, considerable model refinement is necessary to achieve acceptable displacement accuracy. Since singularities are completely absent in the interpolation functions, the tractions near the crack tip can never correctly model physical behavior, even with mesh refinement.

It has been observed that proper placement of certain midpoint nodes in three-dimensional isoparametric finite elements leads to special elements with the appropriate near crack tip displacement and traction variation (Reference 22). A similar element has been developed for the higher order BIE program. The midpoint nodes of the element sides normal to the crack tip are repositioned at the quarter points of the element side, relative to the crack tip. The relationship between the intrinsic coordinate, ξ_1, and r, the physical distance from the crack front, is then (where ℓ = length of element side)

$$\frac{r}{\ell} = \frac{(\xi_1 + 1)^2}{4} \tag{7}$$

The displacements and tractions are quadratic in ξ_1. Using the shape function definitions of Figure 2, it is found that the variation of u_i, t_i in the physical variable is:

$$\begin{Bmatrix} u\ (r) \\ t\ (r) \end{Bmatrix} = A_1 + A_2\sqrt{r} + A_3 r \tag{8}$$

In particular, the crack opening displacement $u_3(r)$ is

$$u_3(r) = A_2\sqrt{r} + A_3 r \tag{9}$$

since $u_3\ (0) = 0$. The modified BIE crack tip element, used on both sides of the crack, thus allows appropriate variation of all displacement components throughout the crack tip region. Since boundary displacements and tractions are independently approximated in the BIE method, this element does not produce the $1/\sqrt{r}$ traction singularity ahead of the crack. This is in contrast to the finite element method in which the quarter point nodal location automatically gives stresses with a $1/\sqrt{r}$ singularity, since they are derived by differentiation of the displacement interpolation functions.

The modified crack tip element has been used for two studies; a part-circular surface crack and a center cracked test specimen.

Figure 3 shows the BASQUE map for the circular crack problem. One-eighth of the body was modeled. The y-z plane was treated as an unmodeled symmetry plane; the x-z plane was modeled to allow solution of the buried or surface crack problem by a change in boundary conditions. Figure 4 compares the crack opening displacements for the buried crack for the standard and modified crack tip elements using both linear and quadratic boundary data variation. The use of the modified crack tip element is seen to give significant improvement in absolute accuracy of displacements, and thus K_I values, for the same map. The use of the modified element causes no increase in computer run time. Figure 5 shows the variation of K_I with crack front location for the surface crack which, as expected, confirms results reported earlier. The impact of the crack tip element is not a change in K_I variation for the surface crack. Rather, it is that the improved absolute accuracy allows direct K_I calculation without resorting to the rather elaborate scaling methods used to connect BINTEQ results to a known analytical solution.

Discussion of the analysis of the center cracked test specimen is deferred until after the description of the traction singularity element.

2.3.2 The Traction Singularity Element

As noted above, the modified crack tip element does not allow singular tractions at the crack tip. It was found possible to modify the BASQUE code to produce the singularity in normal traction on the first element ahead of the crack. The shape functions for traction on this element were modified by multiplication by:

$$\phi(r) = \frac{1}{\sqrt{r}}\left[1 - \frac{r}{\ell}(1-\sqrt{\ell})\right] \tag{10}$$

Because of programming constraints, the modification was actually made in the routines which evaluate the point load solutions. The function $\phi(r)$ is $O(1/\sqrt{r})$ for small values of r and is one at $r = \ell$; thus the singularity is produced and traction continuity is guaranteed on the element boundary at $r = \ell$.

Use of Eq. (10) with a standard element gives

$$\{t\} = \frac{B_1}{\sqrt{r}} + B_2\sqrt{r} + B_3\, r^{3/2} \tag{11}$$

while its use with the modified crack tip element gives

$$\{t\} = \frac{B_1}{\sqrt{r}} + B_2 + B_3\sqrt{r} \tag{12}$$

The higher order terms in the traction expression, Eq. (11), are the appropriate ones. Unfortunately, at the present time one must either use a crack tip element ahead of the crack and accept Eq. (12) or use a standard element and obtain Eq. (11). The former course

has been found to give better results and was used in the study of the center cracked test specimen. The work carried out to date has shown that the traction singularity element has utility which justifies the programming effort required to remove this restriction cited above.

2.3.3 The Center Cracked Test Specimen

The second problem analyzed was that of the center cracked test specimen shown in Figure 6. One-eighth of the geometry was modeled, using two unmodeled symmetry planes but modeling the crack plane. The BIE (BASQUE) maps used in the analysis are shown in Figure 7. Both two-dimensional (plane strain) and three-dimensional analyses were carred out by changing boundary conditions on the plane y = t/2. Singularity finite element results are available for the three-dimensional problem (Reference 23). Attention was given to several different issues, in particular:

1. The effect of the use of crack tip and traction singularity elements;
2. Evaluation of K_I without extrapolation; and
3. Exploration of the region near the crack tip/free surface intersection in the three-dimensional problem.

The specimen was first analyzed in plane strain using Map 1 and a variety of choices of element type and boundary data variation. Figure 8 gives the stress component in the direction of the applied load for the various cases considered. Interior stresses ($\theta = 90°$) were considered as it was found that they were more accurate than the traction values in the crack plane. This result is attributed to the averaging effect of the boundary integral representation for interior stresses. Further, it was intended to use stress, rather than displacement, as the basis for K_I calculations, avoiding any plane stress or plane strain assumptions in the the three-dimensional problem.

Several comments can be made about the results of Figure 8:

1. The use of quadratic variation and crack tip elements gave the best results;
2. The divergence of the finite geometry plane strain (BIE/CRX) solution from the $1/\sqrt{r}$ approximation sets an outer limit (in terms of r/a) to the data to be used in calculating K_I; and
3. The boundary layer effect of finite surface element size on the three-dimensional BIE interior stress calculation sets an inner limit to r/a.

Based on these observations, it was decided to evaluate K_I using the relationship

$$K_I = \sqrt{2\pi r} \left\{ \cos\frac{\theta}{2} \left[1 + \sin\frac{\theta}{2} \sin\frac{3\theta}{2} \right] \right\}^{-1} \sigma_z (r, \theta) \qquad (13)$$

with $\theta = 90°$, $0.01 < r/a < 0.1$. Either point estimates of K_I or an average value of K_I over the interval (in r/a) can be used. In the present study point estimates at r/a = 0.025

and 0.05 were taken because a major objective in the three-dimensional problem was to examine stress behavior as a function of r/a near the free surface.

It must be emphasized that K_I values were not extrapolated back to r/a = 0. Such extrapolation was felt to be inappropriate, at least in the BIE analysis, because of the risk of misinterpreting the numerical boundary layer as a real variation of K_I with r/a. In addition, an extrapolation technique would be especially dangerous near the crack tip/free surface intersection where the nature of the stress singularity is not known. Even ignoring numerical boundary layer effects, the basic information needed to guide meaningful extrapolation does not yet exist.

After the preliminary work done with the relatively crude Map 1, the specimen was analyzed in plane strain using Map 2. Modified crack tip elements were used, both with and without the traction singularity. Table I contains the crack opening displacements for both BASQUE analyses at three different locations through the specimen thickness. The results from a converged BIE/CRX analysis are included as well. There is significant improvement in results near the crack tip due to inclusion of the traction singularity. Further, the results are uniform through the specimen thickness, indicating that the BIE map on the plane y = t/2 is adequately refined.

TABLE I

Ew/σ a : CRACK OPENING DISPLACEMENTS
(PLANE STRAIN)

		3D-Map 2 crack tip element with traction singularity			3D-Map 2 crack tip element without traction singularity		
r/a	Plane strain (BIE/CRX)	y/t = 0	y/t = 0.25	y/t = 0.5	y/t = 0	y/t - 0.25	y/t = 0.5
0.0125	0.399	0.398	–	0.398	0.381	–	0.380
0.05	0.795	0.791	0.792	0.790	0.784	0.785	0.785
0.125	1.243	1.238	–	1.236	1.234	–	1.233
0.2	1.552	1.547	1.547	1.545	1.543	1.544	1.541
0.6	2.444	2.435	–	2.433	2.432	–	2.429
1.0	2.693	2.688	2.688	2.685	2.684	2.684	2.682

The improvement in accuracy due to the traction singularity element carries over to the K_I calculation as well. Table II compares the K_I values obtained with and without the singularity element at r/a = 0.05. The BIE/CRX result given is believed accurate to within 0.25 percent.

TABLE II

$K_I/\sigma\sqrt{\pi a}$ FOR CENTER CRACKED PANEL[1]
(PLANE STRAIN)

Analysis	From Interior Stress ($\theta = 90°$)	From Crack Opening Displacements
BIE/CRX	1.421[2]	1.421[2]
BASQUE – with traction singularity	1.420	1.416
BASQUE – without traction singularity	1.436	1.395

1 – evaluated at r/a ≈ 0.05
2 – evaluated using path independent integral, Reference 21.

It is clear that the use of the traction singularity element improves both the accuracy and the consistency between the stress and displacement fields.

Solution of the three-dimensional problem was carried out using Map 2; later, the more refined Map 3 was also used with no significant change in results. Figure 9 gives nondimensional crack opening displacements for the three-dimensional problem at both the center and free surface of the specimen. Results are given for the BASQUE analysis, the singular finite element analysis of Raju and Newman (Reference 23), and for comparison, for the BIE/CRX solution. The results of the BASQUE analysis show displacements significantly larger than the finite element results at both the center and free surface of the specimen. K_I at the center of the specimen is within 1 percent of the plane strain value.

The effect of the free surface is shown in Figure 10. Stress is plotted as a function of position through the specimen thickness. The BASQUE results are given at r/a = 0.025 and 0.05. The finite element results are based on extrapolation. The BIE and finite element results agree qualitatively, showing an increase in stress, peaking at $y/t \approx 0.42$, followed by a rapid drop off in a boundary layer near the free surface. The BASQUE stress data (at both r/a locations) rise to a higher peak (+ 2.5 percent) closer to the free surface than the finite element data. The BASQUE stresses then drop faster to lower values at the free surface, relative to the singular finite element data.

In addition, comparison of the BIE results at the two different r/a values indicates a possible change in the nature of the stress singularity at the free surface. The behavior of stress near

the peak stress location is consistent with a singularity of higher order than $1/\sqrt{r}$. It is reasonable to suppose, however, that behavior near the crack tip/free surface intersection depends on position relative to both the crack and the free surface. It may well be inappropriate to interpret the data near the free surface simply in terms of distance from the crack tip.

Finally, it is possible that the nature of behavior near a free surface/crack tip intersection cannot be resolved by numerical modeling. In the work discussed here, it has been verified that the behavior shown was not induced by the use of the traction singularity element. Nevertheless, both the BIE and finite element methods assume specific interpolation functions, and these assumptions limit the solution behavior which can be exhibited without excessive mesh refinement. Pending the analytical resolution of the nature of the singularity (if any) at the crack tip/free surface intersection, the most promising approach is the implementation of the flat crack BIE. This approach would completely eliminate the traction modeling problem and allow needed mesh refinement to be concentrated on the more accurate definition of displacements on the free surface and crack near their intersection.

SECTION 3

BIE ANALYSIS FOR INHOMOGENEOUS MATERIALS

3.1 INTRODUCTION

In gas turbine engine applications, inhomogeneous elastic material properties are usually encountered as a result of spatial temperature variation and temperature dependence of elastic material properties. This situation is particularly acute in the combustor and turbine sections of an engine. In these sections, BIE analysis can profitably be applied to turbine blade attachments and the turbine disk rim region using a three-dimensional code and to axisymmetric analysis of a disk using a BIE code such as that described in Reference 24.

The analysis required is a mission analysis; that is, stress analysis of a part must be carried out at several points of the engine operating cycle. The temperature distribution in the part is neither uniform nor steady state at most operating points; thus, effective use of the BIE method requires development of both strategy for efficiently handling the transient thermoelastic problem and a technique for treatment of material inhomogeneity. The remainder of this section discusses possible techniques for the introduction of inhomogeneous elastic material properties in BIE analyses and closes by proposing a strategy which fits the requirements of a mission analysis.

3.2 APPROXIMATE BIE ANALYSIS FOR INHOMOGENEOUS MATERIALS

Even if elastic material properties are assumed to vary in space, Eq. (1) and (2) can still be formally derived. It is not, however, possible to derive an analytical expression for the point load functions U_{ij} (p, Q), T_{ij}(p, Q) for a general inhomogeneous material, even if it is assumed to be isotropic. The absence of such an expression precludes the evaluation of the point load functions by a numerical technique such as that described in the Appendix for homogeneous anisotropic materials. There remain three approaches: derivation of point load solutions for special types of inhomogeneity, material property averaging, and iterative techniques. These approaches are explored in the paragraphs below.

The first possibility, the construction of point load functions for special types of inhomogeneity is attractive in some situations but not in the gas turbine engine environment. It is to be expected that such special point load solutions could be derived only for very simple material property variations, such as linear variation in the spatial variables. This means that, in the solution of any particular problem, the actual material property variation must be approximated using those variations for which special point load functions exist. In gas turbine engine parts the material property variation is not basically spatial, rather it is due to temperature dependence of the elastic material properties and the existance of a highly nonuniform temperature field. This environment leads to a complicated spatial variation of material properties and makes the required approximation difficult if not impossible. This approach is therefore not appropriate for the structural analysis of gas turbine engine parts although it could, at some time, prove useful in other applications.

A second approach is the approximation of the inhomogeneous material by a homogeneous material, using average elastic material properties for the part. The calculation of the average

properties poses no problem, as the normal design process requires thermal analysis of the part prior to stress analysis. The results of an in-house study carried out using an axisymmetric finite element code are discussed below, and these results clearly demonstrate the feasibility of the approach.

The problem studied was the stress analysis of a typical turbine disk under combined centrifugal, thermal, and blade loads. The cross-section of the disk is shown in Figure 11 along with isotherms from the thermal analysis of the disk. The analysis was carried out under two different material property assumptions:

1. E and α (Young's modulus and coefficient of thermal expansion) evaluated based on temperature within each element (Table III).

2. E evaluated at the average disk temperature (567°F) and α at its local value in each element.

Density and Poisson's ratio were held constant, although that is not a necessary restriction. The results of the two analyses are compared for the disk bore and disk rim in Tables IV and V, respectively. The locations at which the comparisons were made are shown in Figure 11.

TABLE III

TEMPERATURE DEPENDENCE OF MATERIAL PROPERTIES

Temperature (°F)	E (psi)	α (in/in/°F)
0	31.25×10^6	6.76×10^{-6}
100	30.75	6.895
200	30.30	7.01
300	29.90	7.13
400	29.50	7.25
500	29.09	7.36
600	28.62	7.46
700	28.19	7.57
800	27.70	7.67
900	27.20	7.78
1000	26.70	7.88
1100	26.19	7.99
1200	25.60	8.11
1300	25.00	8.25
1400	24.40	8.40
1500	23.70	8.62

TABLE IV

EFFECT OF MATERIAL PROPERTY AVERAGING AT DISK BORE

Location	Radial Displacement (in)		Hoop Stress (psi)	
	Analysis 1	Analysis 2	Analysis 1	Analysis 2
B_1	0.01522	0.01526	56,694	58,465
B_2	0.01675	0.01679	82,615	84,604
B_3	0.01833	0.01838	101,069	103,142
B_4	0.01922	0.01925	103,454	105,840
B_5	0.01803	0.01804	84,735	86,663
B_6	0.01647	0.01647	49,759	51,560

TABLE V

EFFECT OF MATERIAL PROPERTY AVERAGING AT DISK RIM

Location	Radial Displacement (in.)		Radial Stress (psi)		Hoop Stress (psi)	
	Analysis 1	Analysis 2	Analysis 1	Analysis 2	Analysis 1	Analysis 2
R_1	0.05583	0.05570	50,424	50,453	–	–
R_2	0.05624	0.05613	50,639	50,644	–	–
R_3	0.05639	0.05629	51,533	51,596	–	–
R_4	0.05636	0.05627	51,545	51,586	–	–
R_5	0.05617	0.05607	50,629	50,618	–	–
R_6	0.05573	0.05563	50,169	50,212	–	–
R_7	–	–	–	–	–17,337	–18,601
R_8	–	–	–	–	–1,818	–2,039
R_9	–	–	–	–	31,687	32,578
R_{10}	–	–	–	–	26,297	27,155
R_{11}	–	–	–	–	14,480	15,023
R_{12}	–	–	–	–	–16,300	–17,022

The good agreement between the two analyses demonstrates the potential of the BIE method in dealing with thermally induced material property inhomogeneity. It should be noted that local evaluation of α is acceptable in the BIE method since it does not enter into the point load functions.

Substructuring could also be used to enhance the accuracy of the material property averaging technique. Reference to Figure 11 shows clearly that decomposition of the disk cross section into two or three appropriately chosen subregions can substantially reduce the difference between extreme and average temperature, and should yield a corresponding increase in accuracy.

Finally, an iterative technique for the inhomogeneous problem has been shown to converge in two-dimensional analysis (Reference 25). To summarize the results, consider the equilibrium equation:

$$\sigma_{ji,i} + X_j = 0; j = 1,3 \tag{14}$$

In the problems considered here, the X_i will normally be the centrifugal and thermal body forces; σ_{ij} is the stress tensor. In the inhomogeneous problem, the terms $\sigma_{ji,i}$ involve non-vanishing space derivatives of both strains (as in the homogeneous case) and material properties. Substituting in Eq. (14) in terms of displacements results in:

$$\frac{1}{1-2\mu}\, u_{i,ij} + u_{j,ii} + \frac{1}{\mu} X_j + F_j = 0 \tag{15}$$

where F_j depends on derivatives of u_i and on the material properties (μ, ν). For a homogeneous material, $F_j = 0$, and Eq. (15) is Navier's equation. The basic result of Reference 25, proved by converting Eq. (15) to an integral equation, is that Eq. 15 can be solved by an iterative technique whose lowest order solution is that for a homogeneous material. Thus, u_i° is the solution of Eq. (15) with $F_j^\circ = 0$. Then F_j^1 is calculated using u_j° and u_j^1 is determined as the solution of:

$$\frac{1}{1-2\nu}\, u_{j,ij}^1 + u_{j,ii}^1 + \frac{1}{\mu} X_j + F_j^1 = 0 \tag{16}$$

Building on this result, a technique for extending the BIE method to inhomogeneous materials is to first solve the problem with homogeneous (average) material properties and then improve this result by calculating the term F_j and applying it as an additional body force term in a second BIE solution. The results cited for the averaging technique alone make it unlikely that more than one or two iterations would be required to achieve acceptable accuracy in practical problems.

3.3 A COMPUTATIONAL STRATEGY FOR TRANSIENT THERMAL ANALYSIS

As was mentioned in Section 1, the presence of body forces, f(q), requires the introduction of a volume integral for each source point P (x),

$$\int_V U_{ij}\,(P,q)\;\; f(q)\; dv \tag{17}$$

in the BIE, Eq. (2). The centrifugal load terms can be converted directly to a surface integral, but, for a time dependent temperature field, the thermal loading term can not be converted. Since time dependent temperature fields are characteristic of mission analysis, an efficient method will be required for the evaluation of Eq. (17). Preliminary studies indicate that the evaluation can be accomplished without undue impact on BIE solution time.

Heat transfer analysis for gas turbine engine parts is typically conducted by using methods which subdivide the region into a finite number of two- or three- dimensional elements, B_k, each of which has a single assigned value of temperatue, T_k. Heat transfer analysis is normally carried out prior to stress analysis so that the geometrical subdivision of the part and the time dependent temperatures are known to the stress analyst. The use of the explicit expression for the point load function U_{ij} allows Eq. (17) to be rewritten (see Reference 4) as:

$$\int_V F(\alpha, E, \nu)\, G(P, q)\, T\ (q)\, dv \tag{18}$$

where α is the coefficient of thermal expansion, E is Young's modulus, ν is Poisson's ratio, T (q) is the temperature field and G (P,q) is a known function involving derivatives of the point load function U_{ij}. The expression can then be expanded as:

$$\sum_{k=1}^{M} \int_{B_k} F(\alpha, E, \nu)\, G(P,q)\, T_k(q)\, dv \tag{19}$$

Since temperature is constant within each element, Eq. (19) can be evaluated as:

$$\sum_{k=1}^{M} F(\alpha_k, E_k, \nu_k) T_k \int_{B_k} G(P,q)\, dv \tag{20}$$

The calculation of Eq. (20), using a numerical volume integration technique, is expensive,but it is required only once since the individual integrals do not involve temperature. Once the integrals are available, they can be used repeatedly to generate the thermal load vector for as many time points as desired. Further, incorporation of temperature dependence in α is straightforward, since it occurs outside the integral sign in Eq. (20). The temperature dependence of E can be handled using the averaging technique described in Section 3.2.

Preliminary estimates indicate that the overhead cost for including transient thermal analysis should be 50 to 100 percent relative to the same problem under mechanical loads alone, but that the added cost for each additional time point should be under 5 percent. This cost makes the technique attractive relative to finite element methods.

REFERENCES

1. Cruse, T. A., "An Improved Boundary-Integral Equation Method of Three-Dimensional Elastic Stress Analysis," *Comp. & Struct.*, 4, 741-754 (1974).

2. Cruse, T. A., "Mathematical Foundations of the Boundary-Integral Equation Method in Solid Mechanics," AFOSR-TR-77-1002, Accession Number ADA 043114, July 1977.

3. Cruse, T. A., Osias, J. R., and Wilson, R. B., "Boundary-Integral Equation Method for Elastic Fracture Mechanics Analysis", AFOSR-TR-76-0878, Accession No. ADA 027716 (1976).

4. Cruse, T. A., "Boundary-Integral Equation Method for Three Dimensional Elastic Fracture Mechanics Problems". AFOSR-TR-75-0813 (1975).

5. Osias, J. R., Wilson, R. B. and Seitelman, L. H., "Combined Boundary–Integral Equation/Finite Element Analysis of Cracked Solids," *Proceedings of the International Symposium on Innovative Numerical Analysis in Applied Engineering Science*, Versailles, France, May 23-27, 1977.

6. Cruse, T. A., Meyers, G. J., and Wilson, R. B., "Fatigue Growth of Surface Cracks," *Flaw Growth and Fracture*, ASTM STP 631, American Society for Testing and Materials, 1977, pp. 174-189.

7. Cruse, T. A. and Meyers, G. J., "Three-Dimensional Fracture Mechanics Analysis," *Journal of the Structural Division;* American Society of Civil Engineers, Vol. 103, No. ST2, Feb. 1977, pp. 309-320.

8. Cruse, T. A. and Wilson, R. B., "Advanced Applications of Boundary-Integral Equation Methods," *Nucl. Eng. and Des.*, to appear.

9. Cruse, T. A. and Wilson, R. B., "The Use of Singularity Functions in Boundary-Integral Equation Fracture Mechanics Modeling," *Proceedings of the 14th Annual Meeting of the Society of Engineering Science, Inc.*, Bethlehem, Pa., Nov. 14-16, 1977.

10. Rizzo, F. J., "An Integral Equation Approach to Boundary Value Problems of Classical Elastostatics," *Q. Appl. Math.*, 25, 83-95 (1967).

11. Cruse, T. A., "Numerical Solutions in Three Dimensional Elastostatics", *Int. J. Sol. Structures*, 5, 1259-1274 (1969).

12. Lachat, J. C., and Watson, J. O., "A Second Generation Boundary Integral Equation Program for Three-Dimensional Analysis," in *Boundary-Integral Equation Method*, ASME, 85-100 (1975).

13. Cruse, T. A., "An Improved Boundary-Integral Equation Method for Three Dimensional Elastic Stress Analysis", *J. Comp. Struct.*, 4, 741-754 (1974).

14. Rizzo, F. J. and Shippy, D. J., "Thermomechanical Stress Analysis of Advanced Turbine Blade Cooling Configuration", AFOSR-TR-76-0841, Accession No. ADA 027718 (1976).

15. Synge, J. L., *The Hypercircle in Mathematical Physics,* Cambridge University Press, 1957.

16. Vogel, S. M. and Rizzo, F. J., "An Integral Equation Formulation of Three-Dimensional Anisotropic Elastostatic Boundary Value Problems," *J. Elas.*, Vol. 3, No. 3 (1973).

17. Rice, J. R., *International Journal of Solids & Structures,* Vol. 8, 1972, pp. 751-758.

18. Cruse, T. A. and Besuner, P. M., *Journal of Aircraft,* Vol. 4, 1975, pp. 369-375.

19. Snow, J. R., "Stress Intensity Factor Calibration for Corner Flaws at an Open Hole," Technical Report AFML-TR-74-282, Air Force Materials Laboratory, Dayton, Ohio, 1974.

20. Cruse, T. A., "Application of the Boundary-Integral Equation Method to Three Dimensional Stress Analysis", *J. Comp. Structures,* 3, 509-527 (1973).

21. Snyder, M. D. and Cruse, T. A., "Boundary-Integral Equation Analysis of Cracked Anisotropic Plates", *Int. J. Fracture,* 11, 315-328 (1975).

22. Barsoum, R. S., "On the Use of Isoparametric Finite Elements in Linear Fracture Mechanics," *Int. J. Numer. Methods Eng.* Vol. 10, No. 1, 1976, pp. 25-37.

23. Raju, I. S. and Newman, J. C., Jr., "Three-Dimensional Finite Element Analysis of Finite Thickness Fracture Specimens," NASA TN D-8414, May 1977.

24. Cruse, T. A., Snow, D. W., and Wilson, R. B., "Numerical Solutions in Axisymmetric Elasticity," *Comp. & Struct.*, 7, 445-451 (1977).

25. Aleksandrovich, A. I., "The Plane Inhomogeneous Problem in Elasticity Theory", *Mekhanika,* 28, 52-59 (1973).

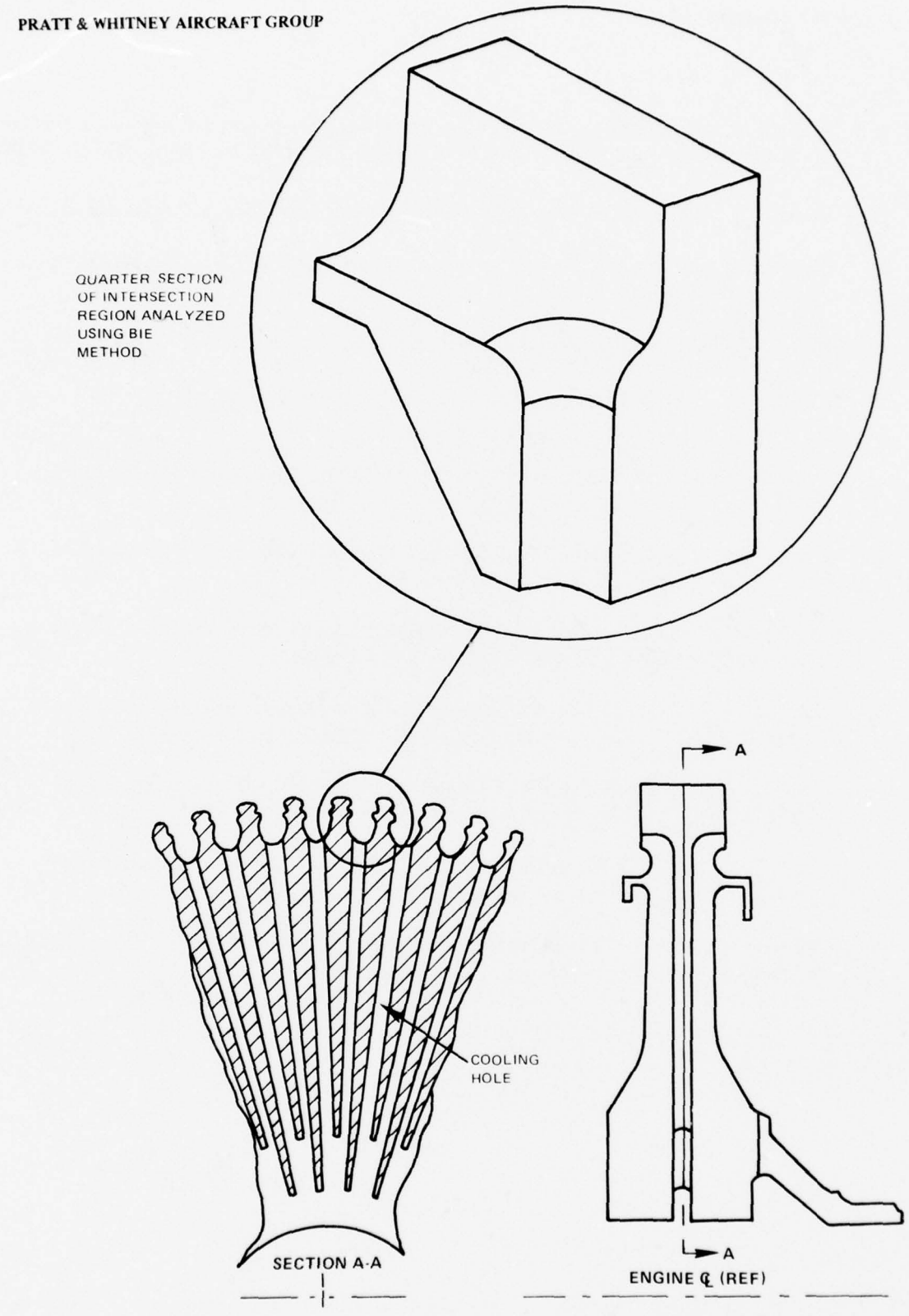

Figure 1a Turbine Disk Rim Slot/Cooling Hole Intersection

MODEL USING 97 QUADRATIC ISOPARAMETRIC ELEMENTS

MODEL USING 436 PLANE TRIANGULAR ELEMENTS

Figure 1b BIE Maps for Analysis of Turbine Disk Rim Slot/Cooling Hole Intersection

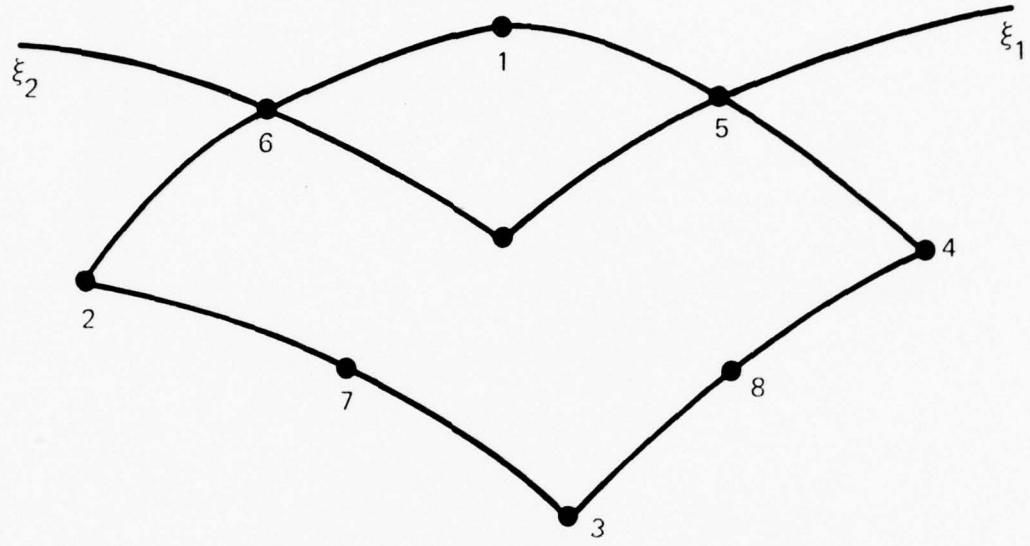

$$X_i(\xi) = M^{\alpha}(\xi)\, X_i^{\alpha} \qquad \alpha = 1, 2, \cdots, 8$$

$$M^1(\xi) = \tfrac{1}{4}(\xi_1 + 1)(\xi_2 + 1)(\xi_1 + \xi_2 - 1)$$

$$\vdots$$

$$M^5(\xi) = \tfrac{1}{2}(\xi_1 + 1)(1 - \xi_2^2)$$

$$\vdots$$

Figure 2 Quadratic Isoparametric Shape Functions

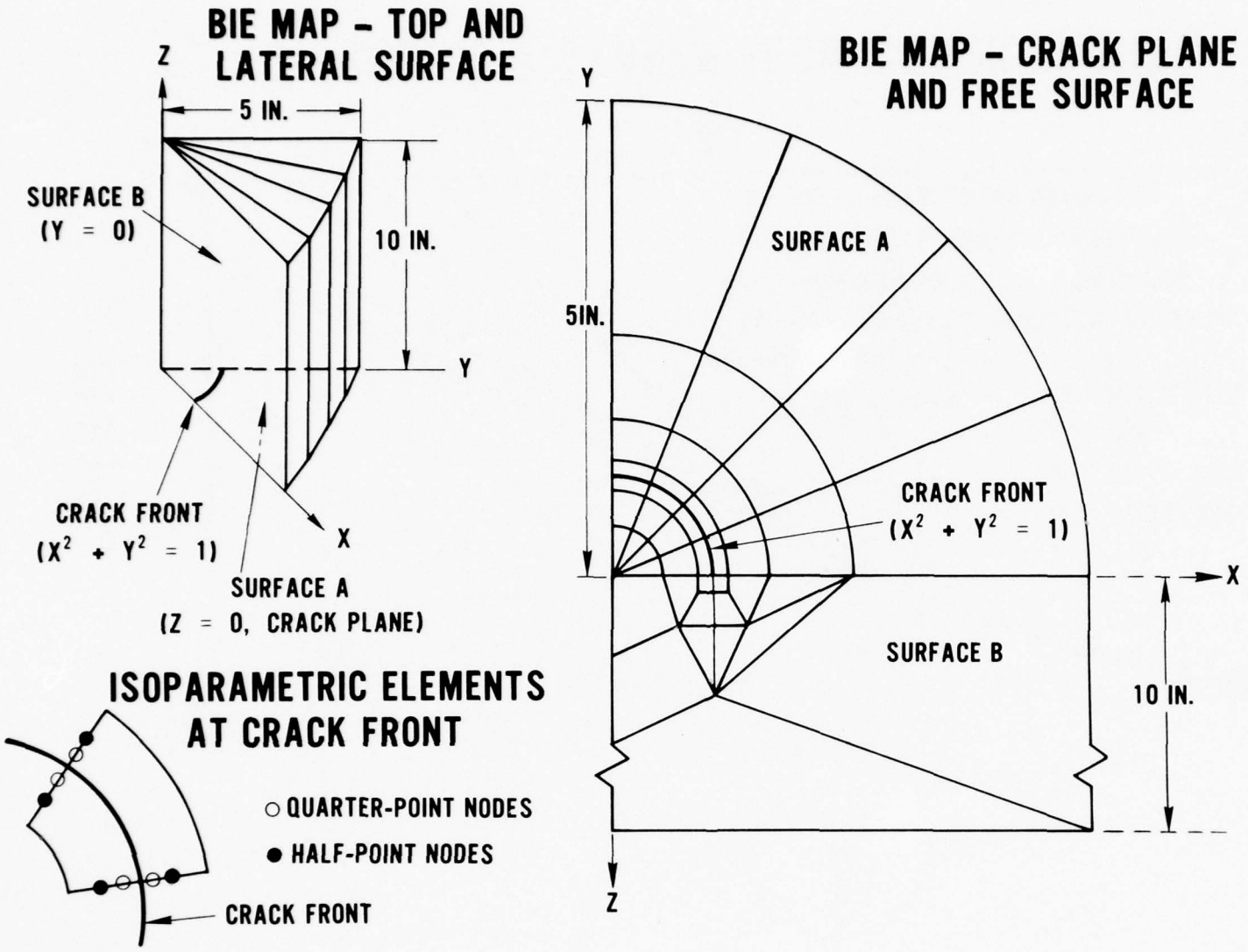

Figure 3 *Boundary-Integral Equation Map for a Circular Crack*

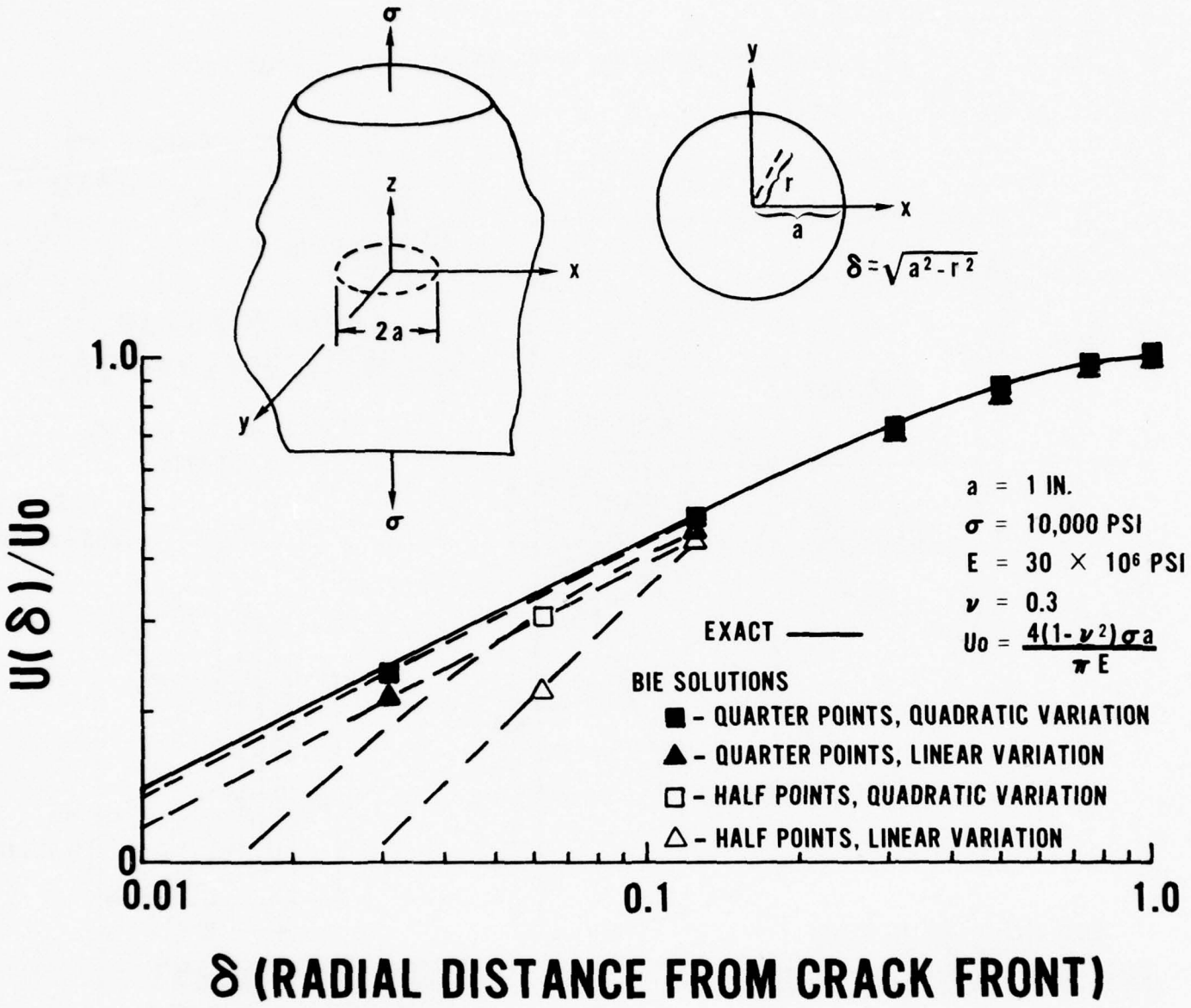

Figure 4 Displacement Variation for a Buried Circular Crack

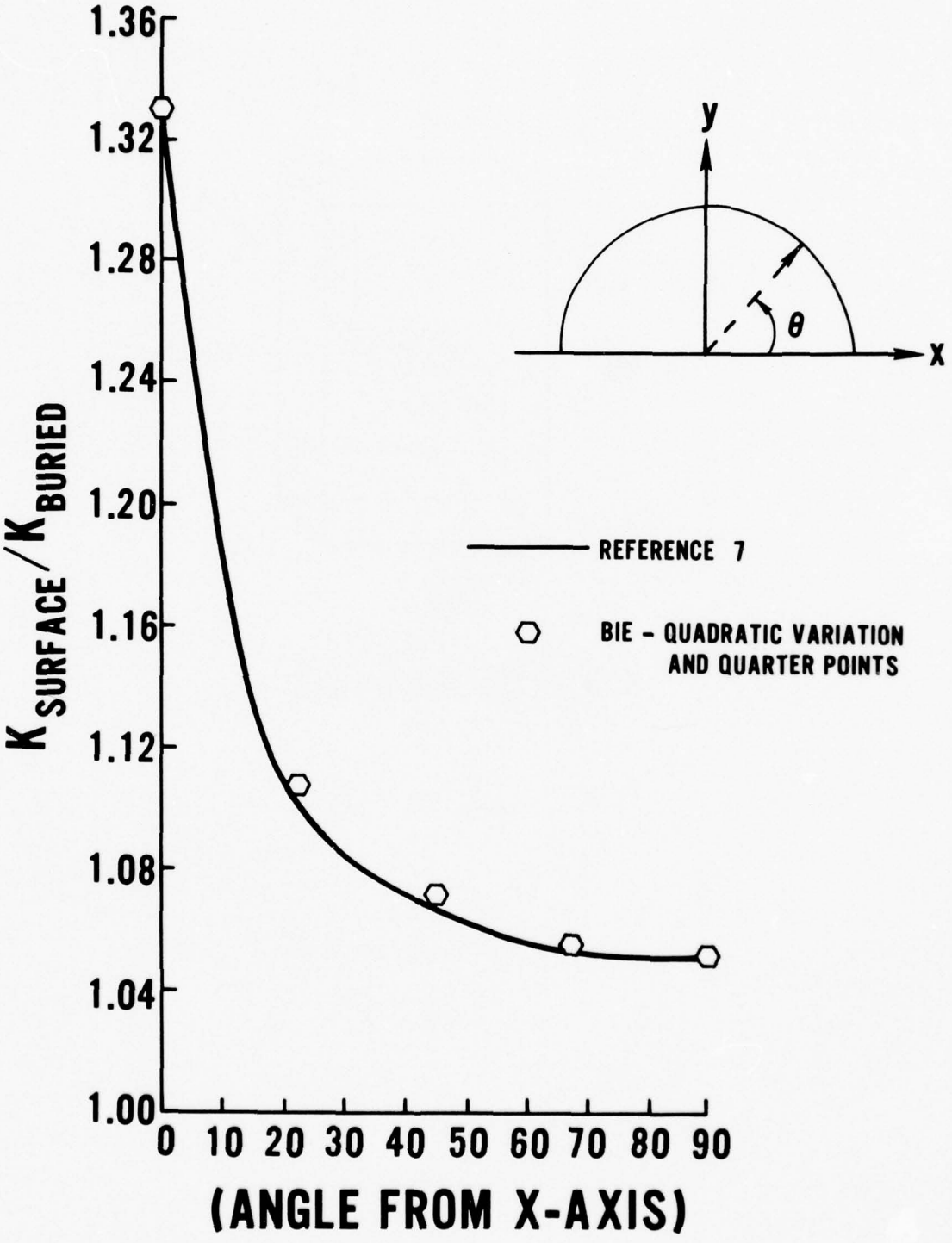

Figure 5 Stress Intensity Factor Variation for a Semicircular Surface Crack

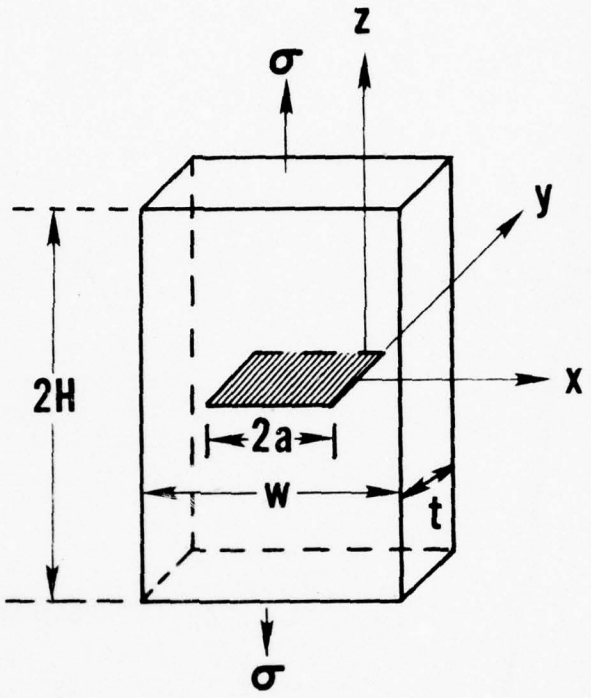

$H/a = 1.75;\ 2a/w = 0.5$

$t/w = .75;\ \nu = 1/3$

Figure 6 Center Cracked Test Specimen

Figure 7 BIE Maps of One – Eighth of Center Cracked Test Specimen

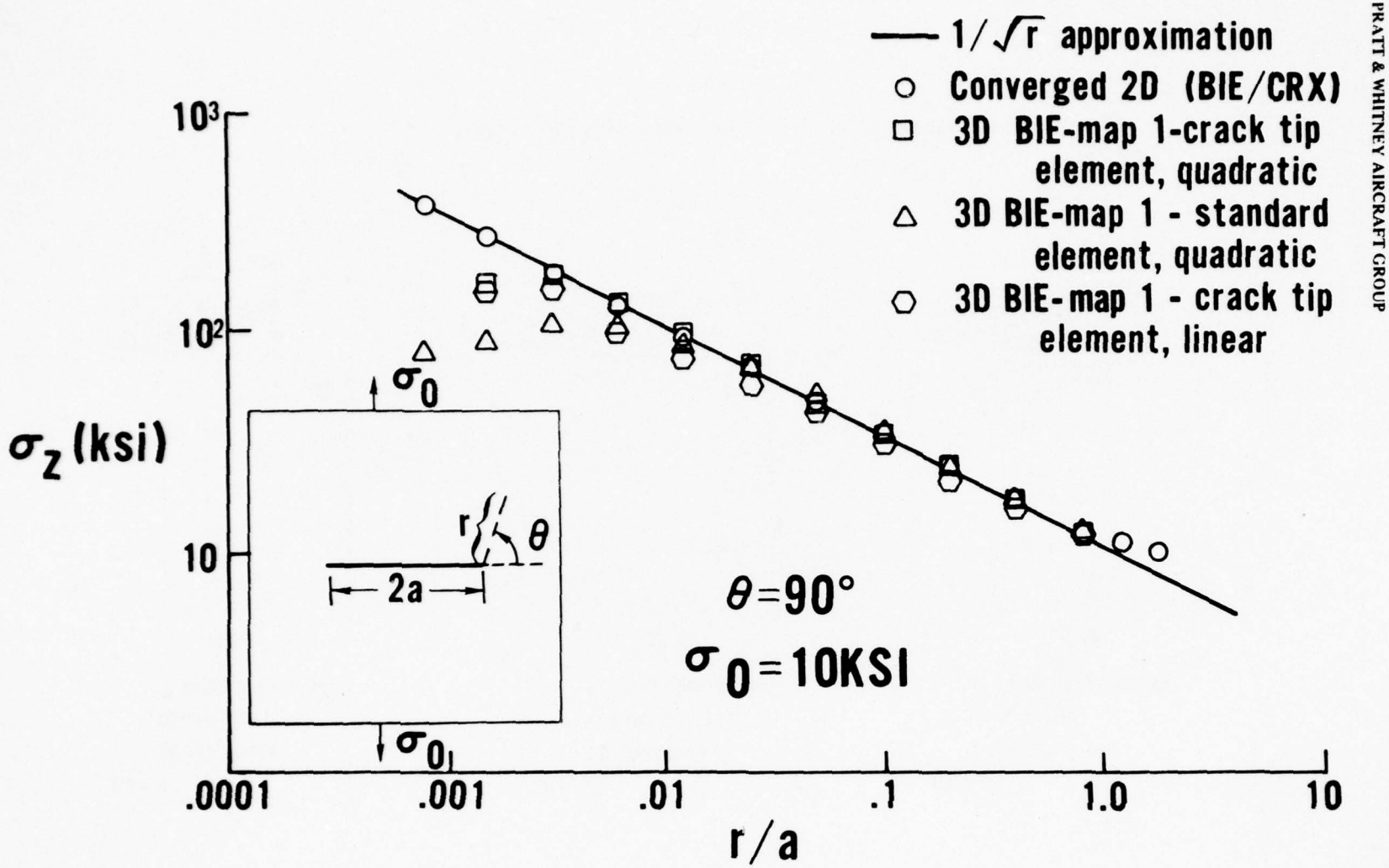

Figure 8 Effect of Modified Crack Tip Element On Interior Solution

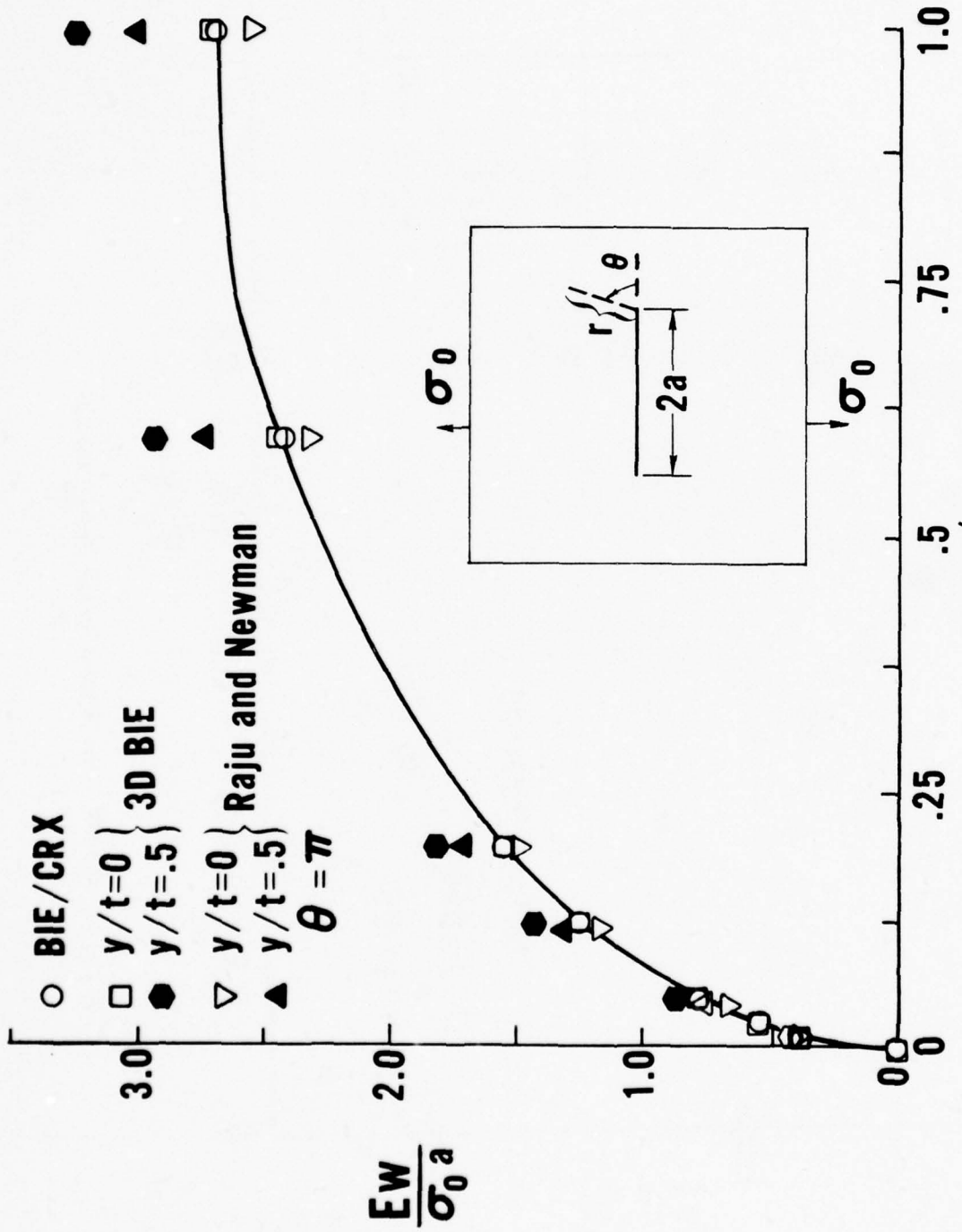

Figure 9 Crack Opening Displacement In the Three-Dimensional Problem

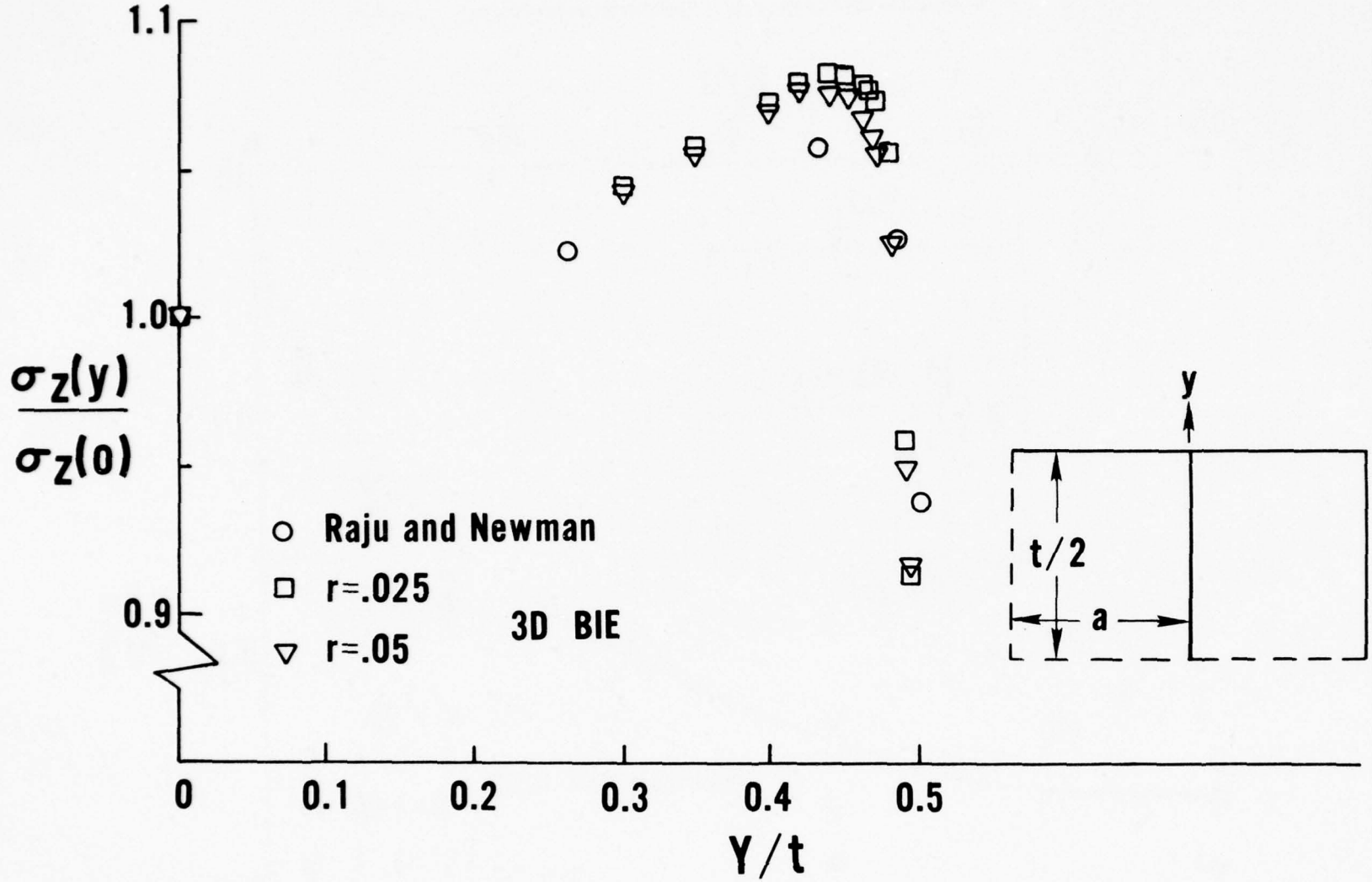

Figure 10 Stress Variation Through Specimen Thickness

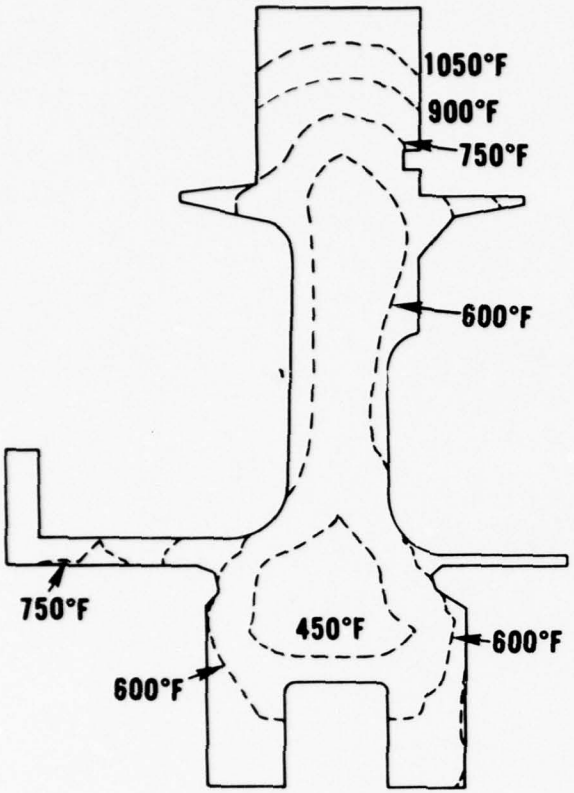

Isotherm map

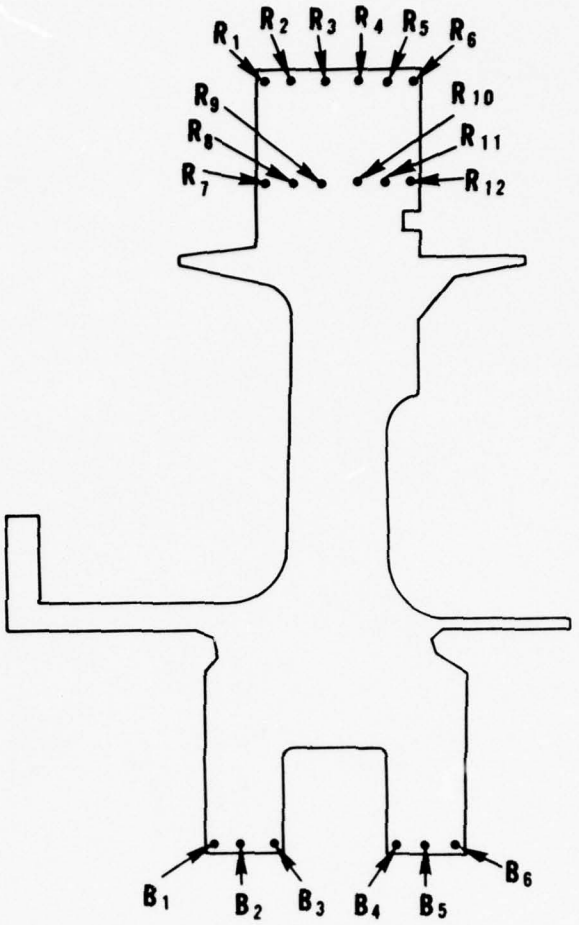

Points for stress and displacement comparison

Figure 11 Radial Section of Turbine Disk

APPENDIX

EFFICIENT IMPLEMENTATION OF ANISOTROPIC THREE DIMENSIONAL BOUNDARY-INTEGRAL EQUATION *STRESS ANALYSIS*

R. B. Wilson and T. A. Cruse

Engineering Department
Commercial Products Division
Pratt & Whitney Aircraft Group
East Hartford, Connecticut
U.S.A. 06108

Accepted for Publication
in the
International Journal for
Numerical Methods in Engineering

SUMMARY

The boundary-integral equation method is particularly well suited for solution of stress concentration and elastic fracture mechanics problems. The method was not previously applicable to anisotropic three dimensional problems because no efficient technique existed for calculation of the required point load solution for an infinite body. A technique has been developed to evaluate numerically the anisotropic point load solutions, and used to generate data bases for various materials. An interpolation technique is used to evaluate the point load solutions efficiently within a higher order boundary-integral equation code. The effectiveness of the technique is verified by solution of problems involving both uni-axial stress states and stress concentrations.

INTRODUCTION

Increasing structural use is being made of materials with anisotropic elastic material properties. Composites have been used with substantial weight advantage in various airframe structures. Eutectic and directionally solidified alloys are finding increasing use in advanced gas turbine engines to provide increased strength without weight and performance penalties.

The elastic stress analysis required for such anisotropic materials falls generally into one of two classes, the general analysis of an entire structure (for example, a disk or turbine vane) or the detailed analysis of a critical subsection. The general stress analysis of a structure does not usually require a precise definition of high stress gradients and can be effectively carried out (in both two and three dimensions) using generally-available stress analysis computer codes.

A detailed and accurate calculation of stresses in regions of rapid stress variation is often required, both for general design purposes and as input for fatigue life calculations.[1] Three-dimensional analysis is often needed to account properly for the effects of part geometry and loading. The boundary-integral equation method is particularly well suited to problems requiring the resolution of high stress gradients.[2] In two dimensions, it already provides a numerical technique applicable to either isotropic or anisotropic materials.[3] This paper describes the extension of the technique to anisotropic three-dimensional elasticity. A method for the numerical calculation of the anisotropic point load solutions is presented and results of boundary-integral equation analyses for several anisotropic materials are discussed.

ANALYTICAL FORMULATION

The Boundary-Integral Equation Method

This paper does not attempt a detailed review of the boundary-integral equation method. For this the reader is referred to Cruse[2] or Lachat and Watson.[4] We simply recall that the method is based on knowledge of the point load solution $U_{ij}(\underline{x}, \underline{y})$ for an infinite body, which gives the displacements at the field point $\underline{y}$ due to a point force applied at the source point $\underline{x}$. Use of the reciprocal work theorem and appropriate limit operations give the boundary-integral equation

$$(1)\quad \frac{u_i(\underline{x})}{2} + \int_S T_{ij}(\underline{x}, \underline{y})u_j(\underline{y})ds(\underline{y}) = \int_S U_{ij}(\underline{x}, \underline{y})t_j(\underline{y})ds(\underline{y})$$

where T_{ij} is the traction point load solution derived from U_{ij} and u_i, t_i are the boundary data on the region S. Appropriate numerical modeling of u_i, t_i and S then reduces (1) to a set of linear algebraic equations. One of the major advantages of the method, apparent from (1), is that no interior idealization of the body is required. Stresses and displacements at selected interior points can be evaluated by surface integration after the boundary solution is completed.

Anisotropic Point Load Solutions

For three-dimensional isotropic elasticity the point load function $U_{ij}(\underline{x}, \underline{y})$ is the well known Kelvin solution.

$$(2a)\quad U_{ij}(\underline{x}, \underline{y}) = \frac{1}{4\pi\mu|\underline{x}-\underline{y}|}\left\{\frac{(3-4\nu)}{4(1-\nu)}\delta_{ij} + \frac{1}{4(1-\nu)}\frac{(x_i-y_i)}{|\underline{x}-\underline{y}|}\frac{(x_j-y_j)}{|\underline{x}-\underline{y}|}\right\}$$

For a general anisotropic material the point load solution can be represented[5, 6] as

$$(2b)\quad U_{ij}(\underline{x}, \underline{y}) = \frac{1}{8\pi^2|\underline{x}-\underline{y}|}\oint_{|\xi|=1} K_{ij}^{-1}(\xi)ds.$$

The line integral is taken on the unit circle in the plane normal to $(\underline{x}-\underline{y})$ *and passing through* $\underline{x}$. The function K_{ij}^{-1} is

$$(3)\quad K_{ij}^{-1}(\xi) = \left[C_{ijkm}\xi_k\xi_m\right]^{-1}$$

where the C_{ijkm} are the elastic constants of the material. Representations for the traction point load solution T_{ij} can be derived from (2a) or (2b). The representation (2b) of U_{ij}, and the associated T_{ij}, are not directly computable. The extension of the boundary-integral equation method as an effective numerical technique for three-dimensional anisotropic problems requires an accurate and efficient means for calculating the anisotropic point load solutions.

EVALUATION OF ANISOTROPIC POINT LOAD SOLUTIONS

Reduction of Point Load Solutions to Computable Form

The representation (2b) cannot generally be evaluated in closed form. For an isotropic material it reduces analytically to the well-known Kelvin form.[7] The only other case for which a closed-form solution is available is that of a transversely isotropic material.[8,9,10]

A second approach involves series expansions of (2b) and its associated traction solution. A uniformly convergent expansion has been obtained[11], but is not suitable for extensive computation.

The remaining alternative is a direct numerical evaluation of the functions, U_{ij} and T_{ij}. One approach to this problem is indicated by Vogel and Rizzo[7], but the method discussed is quite complex, especially for the function T_{ij} and would be too time consuming for routine numerical use.

The present approach to the calculation of U_{ij} and T_{ij} is based on defining the modulation function,

$$(4) \qquad G_{ij}(v_1, v_2) = \oint_{|\xi| = 1} K_{ij}^{-1}(\xi) ds$$

where v_1, v_2 define the orientation of the vector $\underline{x}$-$\underline{y}$. Then

$$(5) \qquad U_{ij} = \frac{1}{8\pi^2 |\underline{x}-\underline{y}|} G_{ij}$$

As was observed in[7] all the singular behavior of U_{ij} occurs in the first factor; further G_{ij} is independent of $|x-y|$. The evaluation of T_{ij} (the traction point load solution) using Hooke's Law requires the calculation of the displacement gradients $U_{ij,k}$. They can be expressed as

$$(6) \qquad U_{ij,k} = \frac{-(x_k - y_k)}{8\pi^2 |\underline{x}-\underline{y}|^3} G_{ij} + \frac{1}{8\pi^2 |\underline{x}-\underline{y}|} G_{ij,\alpha} v_{\alpha,k}$$

The known $|\underline{x}-\underline{y}|^{-2}$ singularity occurs in easily evaluated closed form expressions, including the derivatives $v_{\alpha, k}$. The derivatives $G_{ij, \alpha}$ are all non-singular, with the exception of possible removable singularities induced by the choice of the v_1, v_2 coordinate system. The higher order derivatives needed for interior stress calculations can be similarly expressed.

The modulation function G_{ij} can be calculated by a straightforward numerical evaluation of the line integral(3). The integrand can be expressed, in closed form, as a rational function of degree -2. The key to the evaluation of the derivatives $G_{ij, \alpha}$ is that the integral in (3) can be transformed so that the integration path is independent of the orientation of $\underline{x}-\underline{y}$; as a result the integrand will then depend explicitly on v_1 and v_2. The required derivatives can then be calculated as

$$(7) \qquad G_{ij, \alpha} = \oint_{|\xi| = 1} \tilde{K}^{-1}{}_{ij, \alpha} ds,$$

by differentiation through the integral sign. Transformation of the material constants C_{ijkl} is not required, rather an explicit substitution $\xi_i = f_i(\eta_1, \eta_2)$ is carried out. Further since

$$\tilde{K}_{ij} \tilde{K}^{-1}_{jk} = \delta_{ik}$$

implicit differentiation gives

$$\tilde{K}^{-1}_{ij, \alpha} = -\tilde{K}^{-1}_{ik} \tilde{K}_{kl, \alpha} \tilde{K}^{-1}_{lj}$$

and the only explicit differentiation required is that of the quadratic forms (in η_1, η_2) which are the elements of $\tilde{K}_{ij}$; Any type of numerical differentiation is completely avoided.

Numerical Evaluation of the Modulation Function

The calculations described have been carried out for a variety of materials. The line integrals were evaluated using Simpson's rule. Table 1 shows the convergence of the modulation function as the integration is refined.

TABLE 1

Convergence of Modulation Function*

Points on Contour	G_{11}	G_{13}
8	3.462192×10^{-7}	3.959000×10^{-8}
16	3.664519×10^{-7}	2.933159×10^{-8}
32	3.598752×10^{-7}	2.959600×10^{-8}
64	3.600230×10^{-7}	2.958070×10^{-8}
128	3.600341×10^{-7}	2.958069×10^{-8}

*$\phi = \nu_1 = 22.5°$, $\theta = \nu_2 = 67.5°$; face centered cubic material

In order to test the algorithm for calculating T_{ij}, the tractions for a face centered cubic material were integrated over the surface of a sphere containing the source point. The results, shown in Table 2, demonstrate the recovery of the applied load.

TABLE 2

Resultant Load on Spherical Surface*

Applied Load Direction	Resultant Load Direction		
	X	Y	Z
X	.999897	.000048	.000099
Y	.000030	.999808	−.000147
Z	−.000004	.000004	.999706

*Unit sphere centered at (.1, .2, .3); load point at (0, 0, 0). Face centered cubic material. Numerical integrations: 32 points for line integrals.

The technique outlined above was incorporated in a higher order three-dimensional boundary integral equation code.[4] A few very simple problems were solved to verify the method, but relative computing times were so large that the method was unsuitable for any realistic problem. A further development of the numerical technique to achieve practical computing times is described below.

Application to Large Scale Stress Analysis

The analytical development and numerical results discussed above show clearly that the anisotropic point load solutions can be computed with essentially arbitrary accuracy. The fact that a face centered cubic material was chosen for the initial investigation implies no restriction. The present effort also treats transversely isotropic and orthotropic materials; further, the extension to full anisotropy requires only the algebra to calculate the explicit forms of the integrands in (3) and (6).

The crucial issue in determining the applicability of the boundary-integral equation method to anisotropic problems of engineering interest is that of efficiency. The lack of closed form expressions for the anisotropic kernel functions requires that the kernel function - boundary data integrals in (1) be evaluated numerically. These integrations are typically the most time consuming part of a boundary-integral equation analysis. Using the closed form isotropic kernels, the numerical integrations in the boundary-integral equation code used require an average of .0015 cpu sec. for each integration point, of which only .0001 cpu sec. is required for the actual kernel function calculation. By contrast, a single calculation of U_{ij} and T_{ij} for an anisotropic material by direct integration (using 64 integration points) requires .025 cpu sec. This implies an increase in overall computing times by a factor of 12 to 16, and is clearly unacceptable for any practical problem.

The solution to this problem is the substitution of an interpolation technique for direct numerical integration in the evaluation of U_{ij} and T_{ij}. The technique is suggested by the fact that G_{ij} and its derivatives are all smooth functions of the variables ν_1, ν_2. The method has been implemented and tested for a variety of materials.

G_{ij} and its derivatives were expressed as functions of ϕ and θ (the two angles in spherical coordinates) in order that interpolation could be carried out in a rectangular table

($0 \leq \phi \leq \pi$, $0 \leq \theta \leq \pi$). Table entries were calculated by direct numerical integration using 64 integration points for the line integral evaluations. Interpolation in the tables was carried out using quadratic or cubic Lagrange interpolation.

To verify the interpolation technique, the tractions were again numerically integrated over a sphere. The recovery of the applied unit loads is shown in Table 3. For these tests a 17 x 33 table was used for G_{ij}. The accuracy obtained using the interpolated point load solution is essentially the same as that obtained using the closed form isotropic kernels. In addition, the load recovery for the anisotropic (transversely isotropic) material is equivalent to that for an isotropic material. The overall level of accuracy is slightly less than shown in Table 2 because a coarser integration mesh was used on the sphere.

TABLE 3

Resultant Load on Spherical Surface

i	j	Applied Load	Isotropic - Exact T_{ij}	Isotropic - Quadratic Interpolation	Isotropic - Cubic Interpolation	Transversely-Isotropic Quadratic Interpolation
1	1	1.0	.99860	.99794	.99845	.99874
	2	0	.00007	−.00007	.00005	−.00017
	3	0	−.00017	−.00007	−.00017	−.00002
2	1	0	.00007	−.00014	−.00005	−.00015
	2	1.0	.99870	.99818	.99837	.99917
	3	0	−.00034	−.00014	−.00034	−.00037
3	1	0	−.00020	−.00010	−.00020	−.00009
	2	0	−.00040	−.00020	−.00040	−.00019
	3	1.0	1.00069	1.00150	1.00101	1.00102

Modulation function data bases were generated for a variety of materials and stored on magnetic tape for use by a suitably modified version of the boundary-integral equation program. The table size used was 33 x 65. The time required for the data base generation was 15 cpu min. for each material, including the calculation of all the derivatives $G_{ij,\alpha\beta}$, which would be required for interior stress calculations. The material constants used are shown in Table 4.

TABLE 4

Material Constants for Data Base Generation

Constant[A]	1 – Isotropic E = 18.07 x 10^6 psi ν = .38931	2 – Isotropic E = 18 x 10^6 psi ν = .3	3-Transversely Isotropic Cobalt[B]
C_{11}	36 x 10^6	24.23 x 10^6	44.52 x 10^6
C_{22}	= C_{11}	= C_{11}	= C_{11}
C_{33}	= C_{11}	= C_{11}	51.94 x 10^6
C_{12}	23 x 10^6	10.39 x 10^6	23.93 x 10^6
C_{13}	= C_{12}	= C_{12}	14.94 x 10^6
C_{23}	= C_{12}	= C_{12}	= C_{13}
C_{44}	6.5 x 10^6 ≈ ½ (C_{11} - C_{12})	6.92 x 10^6	10.92 x 10^6
C_{55}	= C_{44}	= C_{44}	= C_{44}
C_{66}	= C_{44}	= C_{44}	10.30 x 10^6 = ½ (C_{11} - C_{12})

	4 - Transversely Isotropic Zinc[B]	5 - Transversely Isotropic	6 - Orthotropic
C_{11}	23.35 x 10^6	49.4 x 10^6	34.05 x 10^6
C_{22}	= C_{11}	= C_{11}	22.24 x 10^6
C_{33}	8.85 x 10^6	38.1 x 10^6	21.75 x 10^6
C_{12}	4.96 x 10^6	34.6 x 10^6	7.05 x 10^6
C_{13}	7.27 x 10^6	9.7 x 10^6	5.76 x 10^6
C_{23}	= C_{13}	= C_{13}	5.21 x 10^6
C_{44}	5.55 x 10^6	14.2 x 10^6	1.00 x 10^6
C_{55}	= C_{44}	= C_{44}	5.00 x 10^6
C_{66}	9.20 x 10^6 = ½ (C_{11} - C_{12})	7.4 x 10^6 = ½ (C_{11} - C_{12})	8.40 x 10^6

Note: A – $\tau_i = C_{ij}e_j$, C_{ij} given in psi

B – Reference 12, p. 278.

Timing studies of the interpolation show that a complete kernel function evaluation requires .0015 cpu sec. using cubic interpolation. Of this time, .0009 sec. is used for the interpolation of the modulation function and .0006 sec. to calculate U_{ij} and T_{ij} from the interpolated data. The computer time required for an arbitrary anisotropic analysis should be about twice that required for an isotropic analysis of the same geometry.

VERIFICATION OF THE ANISOTROPIC BOUNDARY-INTEGRAL EQUATION ANALYSIS

In order to provide final verification of the formulation and numerical treatment of the anisotropic three-dimensional boundary-integral equation stress analysis, the higher order program[4] was modified to use the interpolation technique for evaluating the point load solutions. Two sets of problems were run; the first for uniaxial stress states and the second for stress concentration problems.

Unixial States of Stress

Exact solutions exist for an anisotropic rectangular parallelepiped subjected to simple tension or pure shear.[13] This allows the comparison of anisotropic boundary-integral equation results with exact solutions. A single boundary-integral equation map, shown in Figure 1, was used for all of these test cases. The map was rotated to allow loading to be applied in different directions. The results of these tests are shown in Tables 5 through 8.

InTable 5 it can be seen that, for an isotropic material, the boundary-integral equation method gives completely equivalent results whether closed form or interpolated kernels are used. Further, both sets of results essentially reproduce the exact solution to the problem of simple tension. Tables 6 and 7 show excellent agreement between exact and boundary-integral equation solutions for a transversely isotropic and an orthotropic material. Finally, Table 8 gives results for the case of pure shear ($\tau_6 \neq 0$, $\tau_i = 0$, i = 1, 5). The maximum error for the pure shear cases is less than .05%.

For the problems involving uniaxial stress states solutions using interpolated point load solutions required 1.7 times as long as those using exact point load solutions. All the cases discussed used linear variation of boundary data and the same precision of numerical integration in the generation of the equation system.

TABLE 5

Cube in Uniform Tension - (Isotropic-Material #2)

	Exact Solution	BIE Numerical Kernels	BIE Exact Kernels	Load Direction
U_z/U_{ze}*	1.00000	1.00017	1.00020	Z
U_x/U_{ze}	−.38983	−.38983	−.38983	
U_y/U_{ze}	−.38983	−.38983	−.38983	
U_x/U_{xe}	1.00000	1.00018	1.00020	X
U_y/U_{xe}	−.38983	−.38981	−.38983	
U_z/U_{xe}	−.38983	−.38981	−.38983	
$U_y/_{ye}$	1.00000	1.00018	1.00020	Y
U_x/U_{ye}	−.38983	−.38981	−.38983	
U_z/U_{ye}	−.38983	−.38983	−.38983	

*All displacements are normalized by the exact extension for the applied loading in Tables 5, 6 and 7.

TABLE 6

Cube in Uniform Tension - (Transversely Isotropic-Material #5)

	Exact Solution	BIE Numerical Kernels	Load Direction
U_z/U_{ze}	1.00000	1.00018	Z
U_x/U_{ze}	−.11547	−.11554	
U_y/U_{ze}	−.11547	−.11553	
U_x/U_{xe}	1.00000	1.00016	X
U_y/U_{xe}	−.68464	−.68460	
U_z/U_{xe}	−.08028	−.08016	
U_y/U_{ye}	1.00000	1.00015	Y
U_x/U_{ye}	−.68464	−.68462	
U_z/U_{ye}	−.08028	−.08016	

Cube in Uniform Tension - (Orthotropic-Material #6)

	Exact Solution	BIE Numerical Kernels	Load Direction
U_z/U_{ze}	1.00000	.99998	Z
U_x/U_{ze}	−.12903	−.12921	
U_y/U_{ze}	−.19355	−.19365	
U_x/U_{xe}	1.00000	.99924	X
U_y/U_{xe}	−.27000	−.26968	
U_z/U_{xe}	−.20000	−.19996	
U_y/U_{ye}	1.00000	1.00014	Y
U_x/U_{ye}	−.17419	−.17428	
U_z/U_{ye}	−.19355	−.19357	

TABLE 8

Cube in Pure Shear (X-Y)

Material	$U_y/U_{y_{exact}}$
Isotropic-numerical (Material #2)	.99984
Isotropic- -exact kernels (Material #2)	.99993
Transversely- - Isotropic (Material #5)	.99989
Orthotropic (Material #6)	1.00004

Stress concentration problems

A second set of cases was chosen to test the applicability of the anisotropic analysis to stress concentration problems, since it is in such problems that the boundary-integral equation method finds its engineering application. In addition, these problems exercise the quadratic variation in geometry and boundary data allowed by the computer program used.

The first problem is that of spherical cavity in a cylindrical rod. The geometry and boundary-integral equation map used are shown in Figure 2. Two different comparisons were made for this problem. First the boundary-integral equation code was used to evaluate the stress concentration for an isotropic material over a range of a/w, using both closed form and interpolated point load solutions. The stress concentration (in terms of mean net section stress) is compared to the values of Reference 14 in Figure 3. Both integral equation analyses show excellent agreement with Reference 14. Of particular interest is the fact that the integral equation solution using interpolated point load solutions shows no more sensitivity to changing a/w than that using closed form solutions. This indicates that mapping requirements for anisotropic analysis should be no more severe than for isotropic analysis. It should be noted that, for this problem, more precise integration in the equation generation was required when using interpolated point load solutions than when using closed form solutions. This was also true in the notch problem discussed below. The computer time ratio of 1.7 for the uniaxial problems increased to the range of 2 to 2.5 for these problems. Some further comments on this question will be made in the last section of this paper.

The problem of the spherical cavity was also solved (for $a/w = .05 \approx 0$) for two transversely isotropic materials, cobalt and zinc. The results are compared, in Table 9, to closed form results derived [15] for the limiting case $a/w = 0$.

TABLE 9

Stress Concentration for a Spherical Cavity
in a Transversely Isotropic Cylindrical Rod

Material	K_{TN} Ref. 2	K_{TN} BIE- - Numerical Kernels
Zinc	1.63	1.47
Isotropic (ν = .3)	2.05	2.03
Cobalt	2.31	2.29

Note- - a/w = .05 ($\approx$ 0) for all cases.

As a last test problem the stress concentration was calculated for a deep hyperboloidal notch under tension. A closed form solution to this problem exists [16] for a transversely isotropic material. The geometry and boundary-integral equation map for the problem are shown in Figure 4. The results of the analysis, for one isotropic and three transversely isotropic materials are shown in Table 10. As in previous cases, the boundary-integral equation solutions using closed form and interpolated point load solutions have equivalent accuracy. Further, the level of accuracy is the same for both isotropic and anisotropic materials. Finally, it should be pointed out that the modeling problem in the notch is extremely complex. With the relatively coarse model used the results are sensitive to the precise location of the mid-point nodes indicated in Figure 4, a question which is independent of material anisotropy. More precisely, correct location of these nodes is required to maintain nearly circular cross sections in constant z planes and to ensure that the BIE model of the notch possesses a vertical tangent at the z = 0 section.

TABLE 10

Stress Concentration in a Hyperboloidal Notch

Material	K_{TN} Ref. 3	K_{TN} BIE - - Numerical Kernels	K_{TN} BIE - - Exact Kernels
Zinc	2.30	2.42	- - - -
Nickle Base Alloy	3.32	3.46	- - - -
Isotropic (ν = .3)	3.34	3.45	3.22
Cobalt	4.02	4.16	- - - -

Note - - K_{TN} = maximum axial stress divided by average stress at minimum cross section. Diameter at minimum section = 1.0, notch radius of curvature = .1.

It should be noted that the results for zinc are less accurate than those for the other materials in both stress concentration problems. It is known[16] that certain mathematical properties of the point load solution for zinc differ from those of the other materials used in this study. It is believed that the effect of this difference in the present formulation is to require more accurate numerical integration of (4) for zinc to achieve the same accuracy in the stress concentration factors.

CONCLUSIONS

It has been shown that anisotropic point load solutions can be numerically evaluated with essentially arbitrary accuracy. Further, accurate boundary-integral equation stress analysis can be carried out using these solutions. Use of an appropriate interpolation technique makes the anisotropic analysis feasible for use in engineering applications.

Future work could profitably be directed at further increases in computing efficiency. In particular:

1. It was noted in solving the stress concentration problems that more accurate integration was required when using interpolated point load solutions. It is likely that this is related to slight oscillations in the modulation function induced by the interpolation scheme. Further investigation should allow at least partial resolution of the problem, with the possibility of a significant saving in solution time.
2. There may well exist a better means of reading the modulation function data base. The presently used Lagrange interpolation is a standard technique which incorporates no knowledge of the physics of the problem.
3. A closed form point load solution exists for transversely isotropic materials[10]. For this material class use of the closed form solution may lead to significant time savings.

Finally, more work remains to be done in extending the anisotropic boundary-integral equation analysis to include thermal and rotational body forces, both of substantial importance in engineering applications.

ACKNOWLEDGEMENT

This work was sponsored by United States Air Force Office of Scientific Research Contract F44620-74-C-0060 with Mr. William J. Walker as Program Manager.

REFERENCES

1) T. A. Cruse, G. J. Meyers, and R. B. Wilson, "Fatigue Growth of Surface Cracks," Flaw Growth and Fracture, ASTM STP 631, American Society for Testing and Materials, 1977, pp. 174-189.

2) T. A. Cruse, "An Improved Boundary-Integral Equation Method of Three-Dimensional Elastic Stress Analysis," *Comp. & Struct.*, 4, 741-754 (1974).

3) M. D. Snyder and T. A. Cruse, "Boundary-Integral Equation Analysis of Cracked Anisotropic Plates," *Int. J. Fract.*, 11, 315-328 (1975).

4) J. C. Lachat and J. O. Watson, "A Second Generation Boundary Integral Equation Program for Three-Dimensional Elastic Analysis," in *Boundary-Integral Equation Method: Computational Applications in Applied Mechanics*, ASME, 1975.

5) F. John, *Plane Waves and Spherical Means Applied to Partial Differential Equations*, Interscience, 1955.

6) J. L. Synge, *The Hypercircle in Mathematical Physics*, Cambridge University Press, 1957.

7) S. M. Vogel and F. J. Rizzo, "An Integral Equation Formulation of Three-Dimensional Anisotropic Elastostatic Boundary Value Problems," *J. Elas.*, Vol. 3, No. 3 (1973).

8) J. R. Willis, "The Elastic Interaction Energy of Dislocation Loops in Anisotropic Media, " *Quart. J. Mech. & App. Math.*, Vol. XVIII, Pt. 4, 1965.

9) I. M. Lifshitz and L. N. Rozenweig, *Jour. Exp. Theo, Phys.* 17, 783 (1974).

10) Y. C. Pan and T. W. Chou, "Point Force Solution for an Infinite Transversely Isotropic Solid," ASME Paper No. 76-WA/APM-18, Dec. 1976, New York.

11) M. Kinoshita and T. Mura, "Green's Functions of Anisotropic Elasticity," AEC Contract Report, C00-2034-5, Northwestern University.

12) H. B. Huntington, "The Elastic Constants of Crystals," in *Solid State Physics - Advances in Research and Applications*, V. 7, 1958, Academic Press.

13) S. G. Lekhnitskii, *Theory of Elasticity of an Anisotropic Body*, Holden-Day, 1963.

14) R. E. Peterson, *Stress Concentration Design Factors*, Wiley, New York, 1953.

15) W. T. Chen, "Axisymmetric Stress Field Around Spheroidal Inclusions and Cavities in a Transversely Isotropic Material," *JAM*, Vol. 35, No. 4, Trans, ASME, Vol. 90, Series E, 1968, p. 770-773.

16) W. T. Chen, "Stress Concentration Around a Hyperboloidal Notch under Tension in a Transversely Isotropic Material," *JAM* Vol, 38, No. 1, Trans. ASME, Series E, 1971, p. 185-189.

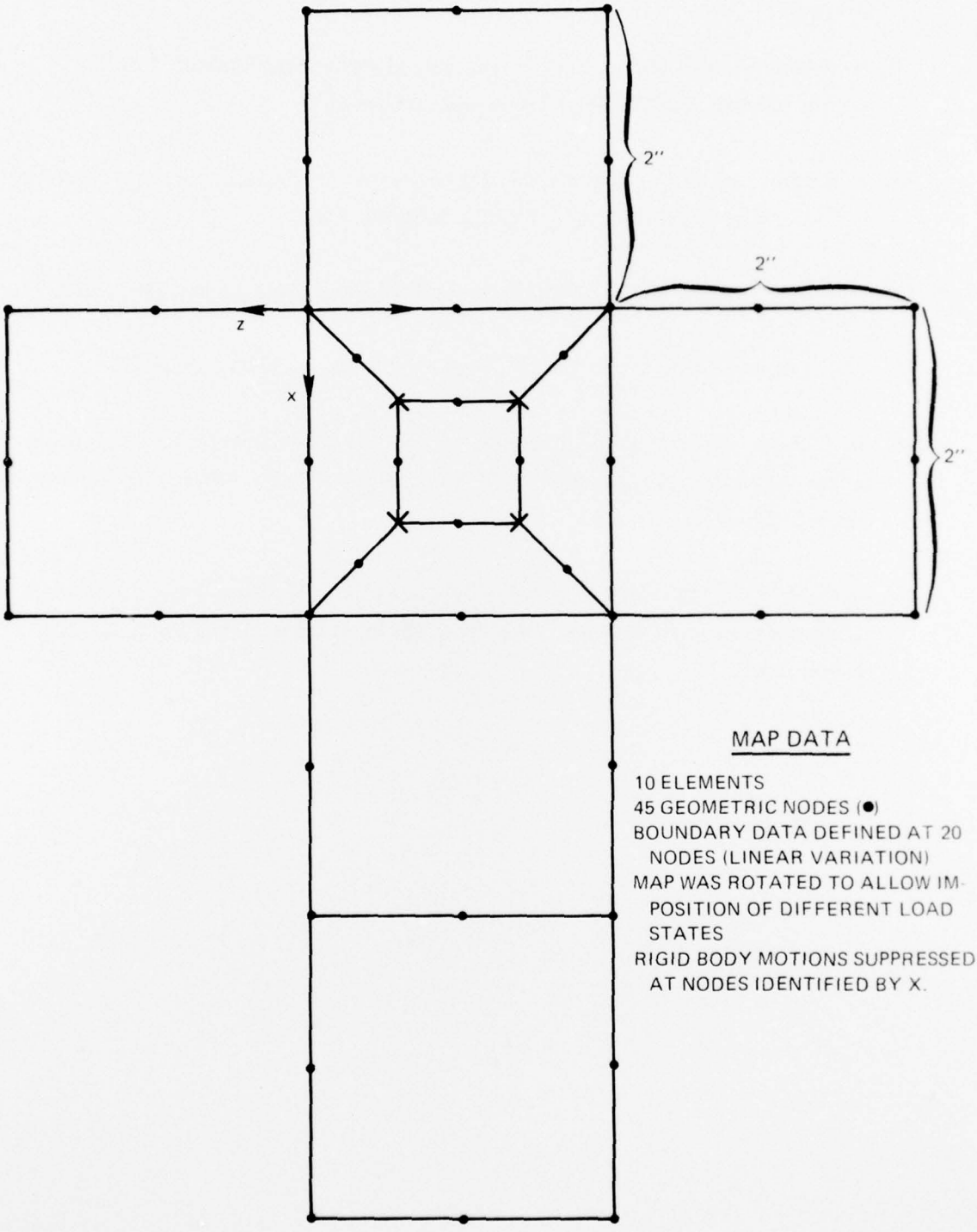

FIGURE 1 BOUNDARY-INTEGRAL EQUATION MAP FOR UNIAXIAL STRESS STATE PROBLEMS

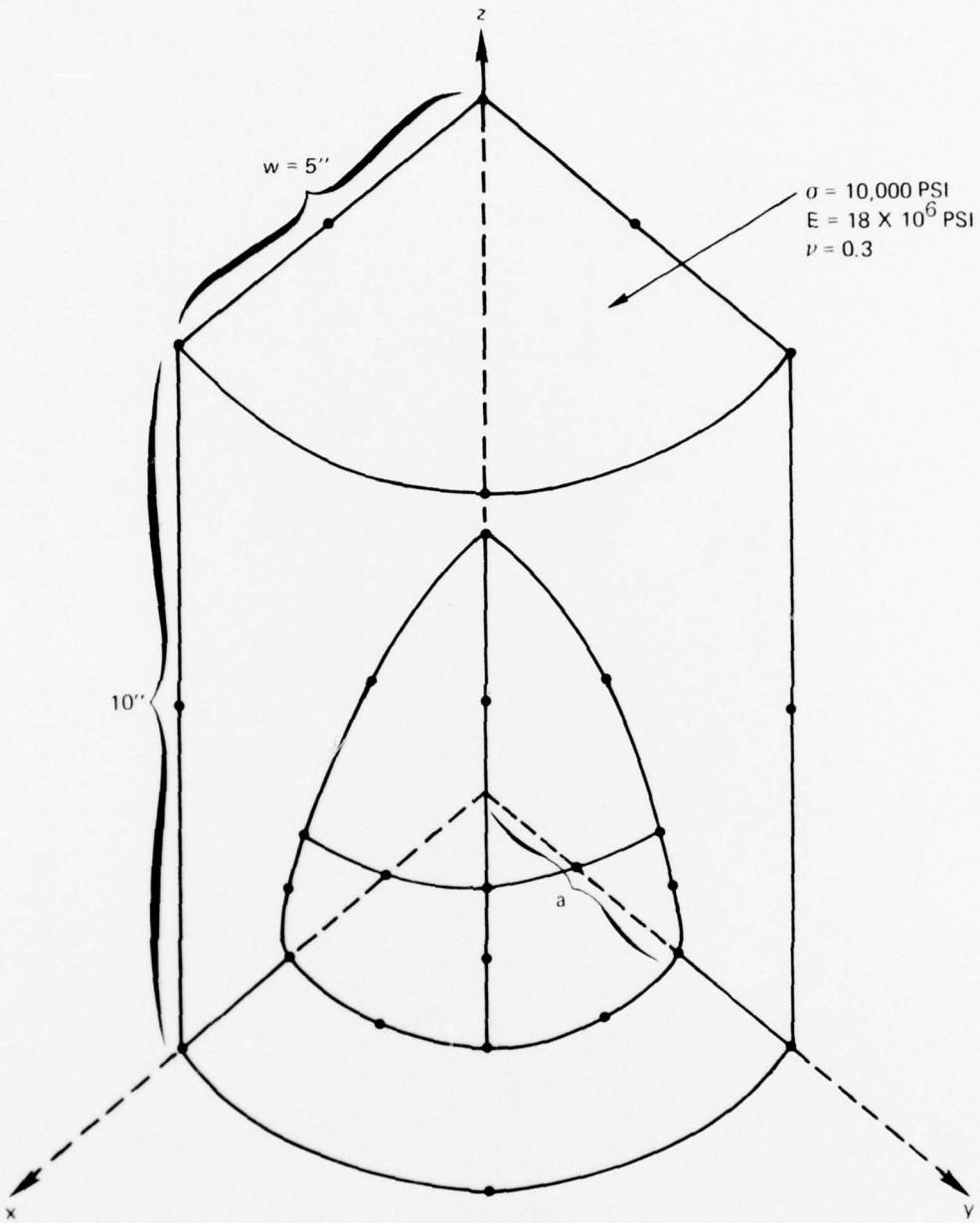

MAP DATA

6 ELEMENTS (CYLINDER-2, CAVITY-4)
28 NODES
QUADRATIC BOUNDARY DATA VARIATION
SYMMETRY WITH RESPECT TO ALL COORDINATES

FIGURE 2 BOUNDARY-INTEGRAL EQUATION MAP FOR SPHERICAL CAVITY

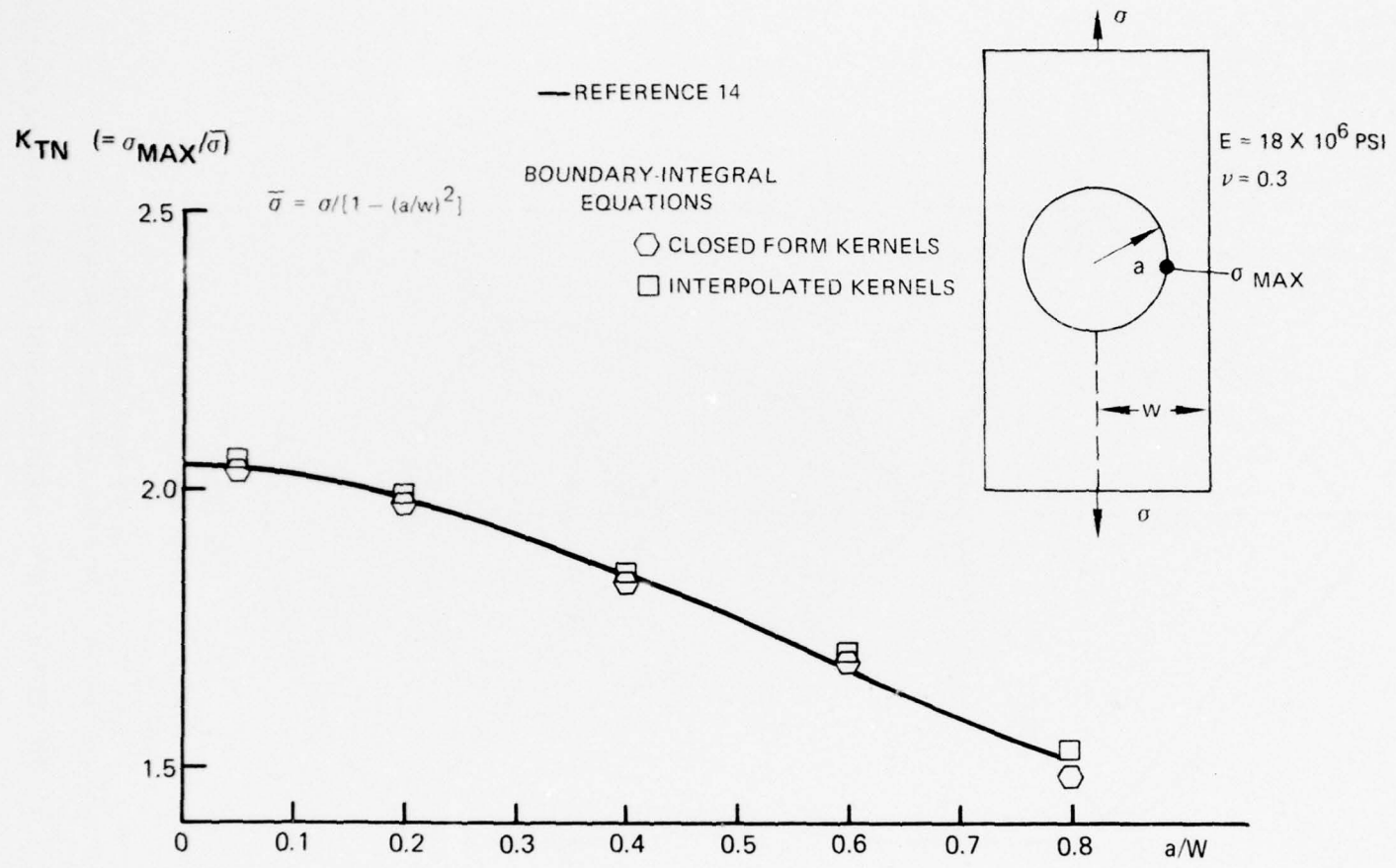

FIGURE 3 STRESS CONCENTRATION FOR A SPHERICAL CAVITY

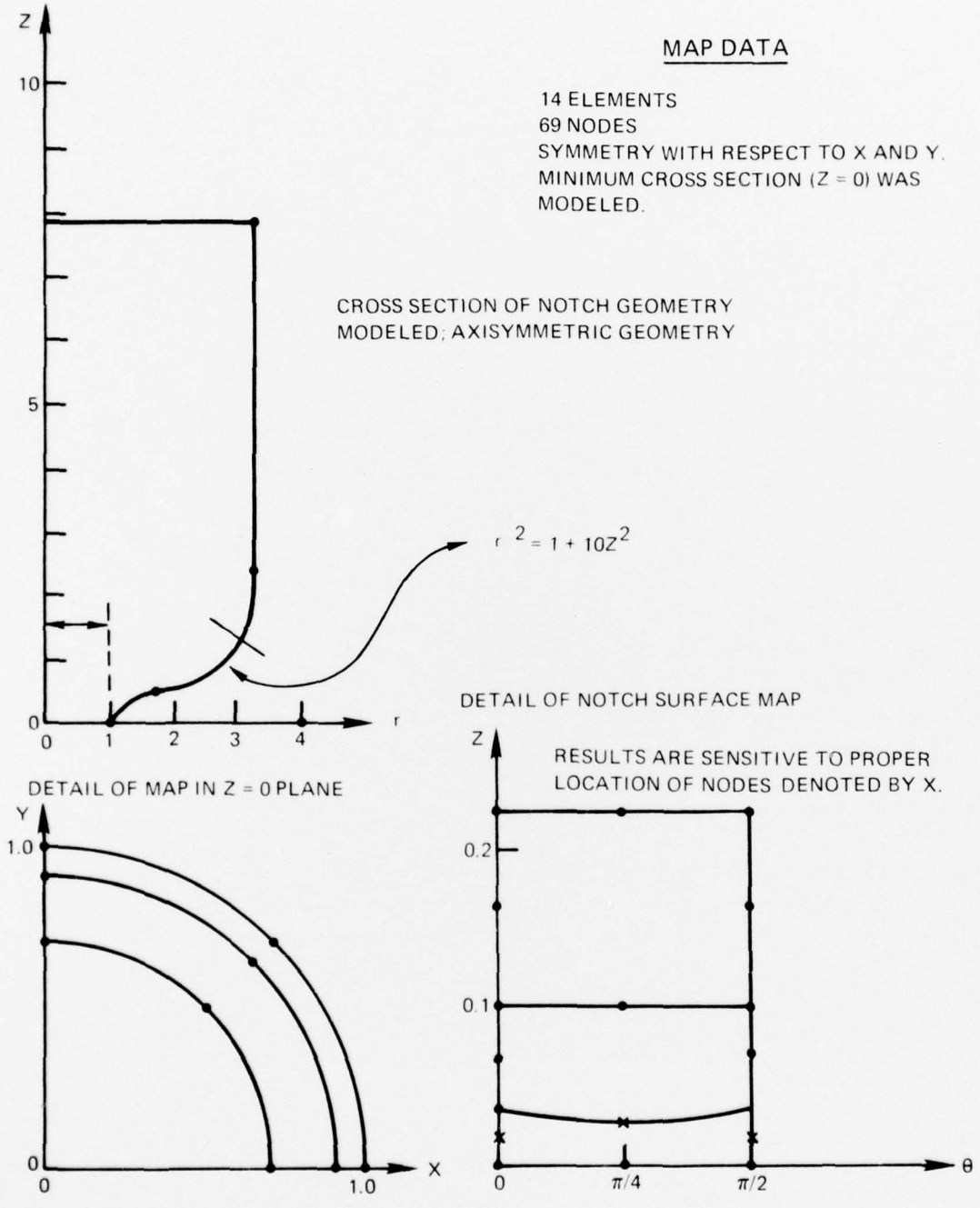

FIGURE 4 BOUNDARY-INTEGRAL EQUATION MAP FOR HYPERBALOIDAL NOTCH